PAGEOPH, Vol. 143, No. 1/2/3 (1994) 0033-4553/94/030317-42$1.50 + 0.20/0

The Frictional Behavior of Lizardite and Antigorite Serpentinites: Experiments, Constitutive Models, and Implications for Natural Faults

LINDA A. REINEN,[1,2] JOHN D. WEEKS[1] and TERRY E. TULLIS[1]

Abstract—Laboratory studies of the frictional behavior of rocks can provide important information about the strength and sliding stability of natural faults. We have conducted friction experiments on antigorite and lizardite serpentinites, rocks common to both continental and oceanic crustal faults. We conducted both velocity-step tests and timed-hold tests on bare surfaces and gouge layers of serpentinite at room temperature. We find that the coefficient of friction of lizardite serpentinite is quite low (0.15–0.35) and could explain the apparent low stresses observed on crustal transform faults, while that of antigorite serpentinite is comparable to other crustal rocks (0.50–0.85). The frictional behavior of both types of serpentinite is well described by a two-mechanism model combining state-variable-dominated behavior at high slip velocities and flow-dominated behavior at low velocities. The two-mechanism model is supported by data from velocity-step tests and timed-hold tests. The low velocity behavior of serpentinite is strongly rate strengthening and should result in stable fault creep on natural faults containing either antigorite or lizardite serpentinite.

Key words: Rock friction, fault mechanics, earthquakes, serpentine, constitutive behavior.

Introduction

The frictional behavior of rocks in a slipping fault zone can influence both the strength of the fault and whether the fault will move by aseismic creep or generate earthquakes. Serpentine is common in many crustal faults including parts of the San Andreas fault (ALLEN, 1968; IRWIN and BARNES, 1975; R. JACHENS, pers. comm.), shear zones in peridotites in the Western Alps (E. H. HOOGERDUIJN STRATING, pers. comm.), and tectonically active regions of the oceanic crust (e.g., CHRISTENSEN, 1972; CANN *et al.*, 1992; TUCHOLKE *et al.*, 1992).

Both continental and oceanic transform faults may be anomalously weak relative to the surrounding crust. For the San Andreas fault, this has been suggested by both the lack of a heat flow anomaly across the fault as well as the nearly

[1] Department of Geological Sciences, Brown University, Providence, Rhode Island, U.S.A.
[2] Now at: Department of Physics and Geology, California State University, Bakersfield, California, U.S.A.

perpendicular orientation of the principal compressive stress direction to the trace of the transform in many areas. Both lines of evidence may indicate low frictional stresses across the fault producing only a small amount of frictional shear heating; this allows the transform to slide at high angles relative to the direction of principal compression. Weakness of oceanic transform faults is suggested by mechanical models for the observed geometries of offset ridge segments (LACHENBRUCH and THOMPSON, 1972; FROIDEVAUX, 1973) and the fact that on the Kane Transform, the axis of least compressive stress is almost perpendicular to the trace of the transform (WILCOCK *et al.*, 1990). The origin of this weakness is unknown, but has been attributed to either the presence of mechanically weak material or over-pressurization of pore fluids within the fault zone.

Petrologic studies of rocks dredged from oceanic transform faults (e.g., AUMENTO and LOUBAT, 1971; BONATTI and HONNOREZ, 1976) reveal a wide variety of rock types including serpentinite, basalt, gabbro, and peridotite. Lizardite is the most common polymorph of serpentine identified on oceanic transform faults (e.g., AUMENTO and LOUBAT, 1971; PRICHARD, 1979; JANECKY and SEYFRIED, 1986). Recent experimental results on lizardite serpentinite indicate that its frictional strength is significantly less than that of other crustal rocks (REINEN *et al.*, 1992d,e). The low frictional strength of lizardite may explain the apparent weakness of transform faults.

Previous researchers have established that measured changes in the frictional response of a rock to instantaneous changes in loading velocity can indicate whether that rock has the potential for stable or unstable slip (e.g., RICE and RUINA, 1983; BLANPIED and TULLIS, 1986; TULLIS, 1988; DIETERICH and LINKER, 1992). This frictional "velocity dependence" of a rock can be measured in the laboratory, and may be used to predict whether a fault will move by aseismic creep or will experience earthquakes. The stability of a slipping fault surface is the result of interactions between the constitutive properties within the fault zone and the elastic loading of the surrounding blocks. If the stiffness of the surrounding material is great, only stable sliding would be expected on the fault. However, in compliant systems (such as the elastic lithosphere and many experimental apparatuses) velocity-weakening behavior can result in unstable, stick-slip events which are analogous to earthquakes.

Empirical constitutive laws have been developed that do a good job of describing both the velocity- and time-dependent frictional behavior of rocks observed in laboratory studies (e.g., DIETERICH, 1979; 1981; RUINA, 1983). These rate- and state-dependent constitutive laws have been applied successfully to experimental results on a wide range of crustal materials over a range of pressure, temperature, and sliding velocity. Recent studies indicate that a multi-mechanism constitutive model is required for serpentinite at room temperature over a range of velocities (REINEN *et al.*, 1992a,c,d), as well as for quartzo-feldspathic rocks under hydrothermal conditions (CHESTER and HIGGS, 1992; BLANPIED *et al.*, 1991).

In this paper we summarize experimental and constitutive modeling results on the frictional behavior of antigorite and lizardite serpentinites, and we discuss the implications for both the strength and sliding stability of natural faults containing serpentine. Our experimental results of antigorite and lizardite gouge support the two-mechanism constitutive model for serpentinite, which was originally developed to model results from velocity-step tests on bare surfaces of antigorite serpentinite. We have analyzed stress relaxation data as an additional piece of evidence in our understanding of the two-mechanism behavior of serpentine.

Two-mechanism Constitutive Model

We model both velocity-step and timed-hold test experimental results using a two-mechanism model that reproduces most of the observed behavior by the interaction of a state-variable constitutive law (SV) dominating at high velocities, and a flow constitutive law (F) dominating at low velocities (see REINEN *et al.*, 1992a). We will use the terms "state-variable mechanism" or "flow mechanism" to refer to the mechanical behavior described by the corresponding constitutive law. These names are for convenience and are not intended to describe the unknown physical processes responsible for the observed mechanical behavior.

The state-variable constitutive law describes both the direct and evolution effects observed at high velocities in serpentinite following changes in velocity. The direct effect, scaled by the constant $\mathbf{a}_{SV}$ in the state-variable constitutive law, describes the initial change in frictional strength in the same sense as the imposed velocity step, while the evolution effect describes the subsequent gradual change in frictional strength to a new steady-state level. We use a two-state-variable form of the Dieterich-Ruina constitutive equations

$$\mu = \mu^*_{SV} + \mathbf{a}_{SV} \ln\left(\frac{V_{SV}}{V^*_{SV}}\right) + \mathbf{b}_1\Psi_1 + \mathbf{b}_2\Psi_2$$

$$\frac{d\Psi_1}{dt} = -\left(\frac{V_{SV}}{D_{c_1}}\right)\left[\Psi_1 + \ln\left(\frac{V_{SV}}{V^*_{SV}}\right)\right] \tag{1}$$

$$\frac{d\Psi_2}{dt} = -\left(\frac{V_{SV}}{D_{c_2}}\right)\left[\Psi_2 + \ln\left(\frac{V_{SV}}{V^*_{SV}}\right)\right]$$

in which the coefficient of friction μ is dependent on both sliding velocity V_{SV} and the state of the sliding surfaces (represented by state variables Ψ_i; $i = 1, 2$). The state variables are scaled by the magnitudes $\mathbf{b}_i$ and evolve over characteristic distances D_{c_i}; μ^*_{SV} is the steady-state friction level at a reference velocity V^*_{SV}.

To describe the behavior which is observed at low velocities, we use a rate-strengthening flow constitutive law with no evolution

$$\mu = \mu_F^* + \mathbf{a}_F \ln\left(\frac{V_F}{V_F^*}\right) \tag{2}$$

in which a direct effect is scaled by $\mathbf{a}_F$ and there is no evolution effect. μ_F^* is the coefficient of friction at reference velocity V_F^*. This constitutive law is equivalent to the exponential flow law often used to model dislocation glide if strain rate is substituted for slip velocity and stress is substituted for μ.

To combine the two constitutive models, we assume that the two frictional mechanisms support the same applied shear load and that the velocity of each mechanism can differ both from each other and from the loading velocity. The total velocity (slip velocity) is the sum of the two velocities:

$$\mu_{\text{observed}} = \mu_{SV} = \mu_F \tag{3a}$$

$$V_{\text{total}} = V_{SV} + V_F. \tag{3b}$$

Combining the state-variable and flow constitutive laws yields

$$V_{\text{total}} = V_{SV}^* \exp\left[\frac{\mu - \mu_{SV}^* - \mathbf{b}_1\Psi_1 - \mathbf{b}_2\Psi_2}{\mathbf{a}_{SV}}\right] + V_F^* \exp\left[\frac{\mu - \mu_F^*}{\mathbf{a}_F}\right]. \tag{4}$$

The frictional velocity dependence of the serpentinites is defined as

$$\frac{\Delta\mu}{\Delta \ln V} = \frac{\mu_1 - \mu_2}{\ln\left(\frac{V_1}{V_2}\right)} \tag{5}$$

where μ_1 and μ_2 are the steady-state friction levels for velocities V_1 and V_2. For the state-variable constitutive law this equals $\mathbf{a}_{SV} - \Sigma\mathbf{b}_i$, and for the flow constitutive law, $\mathbf{a}_F$. Negative values of $\Delta\mu/\Delta \ln(V)$ indicate velocity-weakening behavior which, in a compliant system, can lead to unstable sliding; positive values of $\Delta\mu/\Delta \ln(V)$ are usually associated with stable sliding.

Since the steady-state behavior of the state-variable constitutive law for antigorite serpentinite is rate weakening and the flow constitutive law is rate strengthening (REINEN *et al.*, 1992a), equation (4) produces the steady-state curve in Figure 1a. At high velocities, steady state is a combination of both constitutive laws. At low velocities, both constitutive laws cannot achieve steady state simultaneously and steady state will be represented by only the flow constitutive law (for details, see REINEN *et al.*, 1992a). The constant-state lines show the combined behavior for constant values of the state variables. At high velocities at which the state-variable law dominates, the slope of these lines is $\mathbf{a}_{SV}$. At low velocities equation (2) dominates the behavior; this constitutive law has no state variables, causing the constant-state lines to merge into the flow mechanism line.

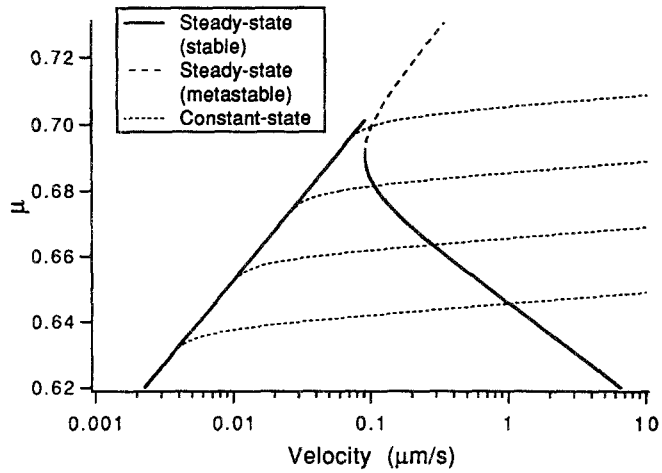

(a)

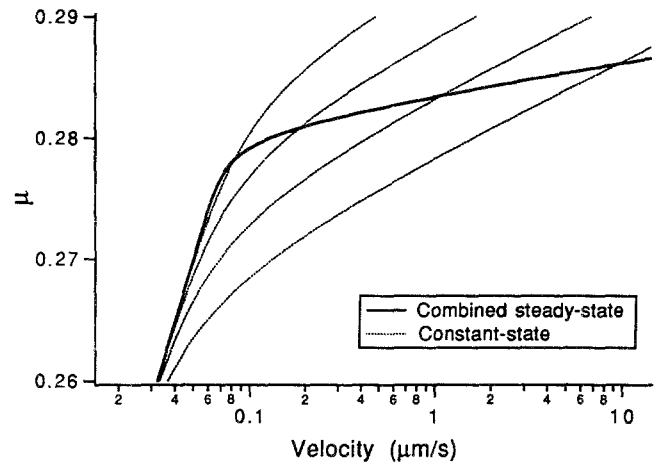

(b)

Figure 1

Combined two-mechanism behavior. (a) Rate-weakening state-variable constitutive law combined with flow constitutive law. The state-variable mechanism dominates combined behavior at high velocities and the flow mechanism dominates at low velocities. The transition to all-flow behavior occurs near 0.1 μm/s for steady-state behavior, and over a range of velocities for constant-state behavior. (b) Rate-strengthening state-variable constitutive law combined with flow constitutive law. The transitional velocities to all flow behavior are nearly the same for both steady-state and constant-state behavior.

Rate-strengthening state-variable behavior is also possible. If the state-variable law is rate strengthening, equation (4) produces the steady-state curve shown in Figure 1b. In this case, the two constitutive laws can both achieve steady-state at all velocities. As with the rate-weakening case, at high velocities at which the state-variable law dominates, the slope of the constant state lines is $\mathbf{a}_{SV}$; at low velocities the constant state lines merge with the flow line and have a slope of $\mathbf{a}_F$. With a

rate-strengthening state-variable law, the constant-state lines merge into the flow line over a smaller velocity range than in the rate-weakening case. We have observed two-mechanism behavior for both cases described here: antigorite exhibits rate-weakening state-variable behavior, and lizardite exhibits rate-strengthening state-variable behavior.

Experimental Details

Experimental Materials

Three different serpentinites were used in this experimental study: GC (primarily antigorite), VM2 (primarily antigorite), and T91NI6 (primarily lizardite). The serpentine polymorphs were determined using X-ray powder diffraction methods described by WHITTAKER and ZUSSMAN (1956), and mineral percentages were determined from thin section analysis.

Dark green serpentinite samples of GC came from a single slab of unknown origin composed of approximately 90% antigorite serpentine, 5% magnetite, and 5% magnesite. The magnesite occurs in veins which were avoided when selecting samples for experiments.

VM2 is an antigorite serpentinite from the Rochester quarry of the Vermont Marble Company. The dark green appearance and the X-ray diffraction pattern of VM2 are very similar to those of the GC serpentinite, however VM2 has small white veins disseminated throughout the sample; these could not be avoided when selecting samples for experiments. X-ray analysis indicates that the small white veins are composed primarily of magnesite with some serpentine fibers.

T91NI6 is a lizardite serpentinite collected from a vein in the Joe Pit mine in the New Idria serpentinite body, California. The pale green appearance and X-ray diffraction pattern of this serpentinite are similar to the lizardite sample (#19–NI–63) collected from the New Idria serpentinite body described in PAGE and COLEMAN (1967). The sample T91NI6 was not large enough to make intact sample rings, and we conducted experiments only on simulated gouge made of this material.

Experimental Procedure

The friction experiments in this study were conducted in a computer-interfaced rotary direct-shear apparatus (TULLIS and WEEKS, 1986). One advantage to using the rotary-shear geometry is the unlimited displacement available, allowing multiple tests on one sample without removing the sample from the pressure vessel. This allowed us to conduct experiments over a range of normal stresses on individual samples, thus eliminating sample variations from our results. In all of our experiments (listed in Table 1), the normal stress and confining pressure were held constant.

Table 1

List of experiments discussed in this paper. Cq is Cheshire quartzite, collected near Middlebury Vermont

Experiment number	Sample rings	Gouge (~1 mm)	σ_N (MPa)	Totd (mm)	Relative dampness†	Date of assembly
fr71	GC	none	25	379	1	11/88
fr81	GC	none	25, 50	60	2	6/89
fr91	GC	none	100, 125	39	2	9/90
fr93	VM2	none	25, 50, 75	85	2	10/90
fr98	VM2	none	25, 75	88	1	4/91
fr101	Cq	GC	25	25	2	8/91
fr104	Cq	GC	25	25	1	1/92
fr105	Cq	GC	25	222	3	1/92
fr109	Cq	T91NI6	25	48	3	6/92
fr114	Cq	T91NI6	25	276	3	9/92
fr117	Cq	T91NI6	25, 50, 75	103	3	11/92
fr127	Cq	T91NI6	25, 50,	103	3	7/93
		75, 100,				
		125, 150				

† Relative dampnesses are 1—assembled in room humidity with no water added to sample surface, 2—assembled in room humidity with distilled water added to sample surface, and 3—assembled in ~100% humidity in glove bag with distilled water added to sample surface.

Normal stress was applied as a combination of confining pressure (84%) and axial load (16%) and ranged from 25 ± 0.8 MPa to 125 ± 1.2 MPa. Confining pressure is known to within 0.1 MPa; the remainder of the uncertainty is in the axial load. Fluctuations in these quantities can be detected with much greater resolution than suggested by the absolute accuracy quoted here; normal stress was held constant to within about 0.1 MPa over a period of a day. In one unjacketed experiment discussed below, normal stress was 25 MPa and was entirely due to axial load. The loading velocities in our experiments ranged from 0.001 to 10.0 μm/s held to within 0.01%. The lowest velocity approaches typical plate motion rates, corresponding to a slip rate of about 32 mm/yr.

We have conducted velocity-step and time-hold tests in our experiments. Velocity-step tests record the change in frictional resistance resulting from a step change in loading velocity. The velocity dependence of the serpentinite is determined from the change in steady-state friction levels before and after the velocity change, normalized by the magnitude of the velocity change (equation (5)). Timed-hold tests record the time-dependent strengthening of contacts on the sliding surfaces. In these tests, the loading velocity is set to zero for a specific amount of time and then reset to the initial value. The transient peak in frictional strength upon reloading is a measure of the time-dependent strengthening of contacts on the sliding surface. During the time the loading velocity is zero, slip at the surfaces continues and the shear stress on the sample relaxes. High-resolution measurement of sample slip is

provided by an internal resolver with a resolution of 0.01 μm at the sample midline and a calibrated accuracy of 0.02 μm (WEEKS *et al.*, 1992). This allows us to determine sample displacement in addition to measuring the relaxation of stress. Sample slip velocity can then be estimated by differencing the slip measurements.

In most of our experiments, sliding was stable and a steady-state coefficient of friction can be measured and used to determine frictional velocity and time dependence. In other experiments, most notably the gouge experiments on antigorite serpentinite at high velocities, displacement in the sample occurred by stick-slip motion. Under these conditions steady-state was not achieved, however a pseudo-steady-state behavior is observed in which the range of stress drops remains constant with time and the range of friction measured during these stress drops can be recorded. In this paper, we do not report velocity dependence values from portions of experiments which were undergoing stick-slip sliding. We do however use stress-relaxation data from hold tests initiating from stick-slip sliding. In timed-hold tests, we assume that the state is the same at the initiation of each hold test. Once an apparent steady state is achieved, the loading velocity is set to zero and the timed hold begins. WEEKS and TULLIS (1992) have shown that by artificially increasing the stiffness of the system through servo-control, stable sliding can be achieved on samples which are unstable at the natural stiffness of our machine. For such servo-control to be successful, the transients in frictional resistance that occur with velocity changes must occur slowly enough for the control system to respond; this places a lower limit on D_{c_1} in a servo-controlled system. We attempted to servo-control slip in the serpentine experiments and found D_{c_1} too small to successfully use this method.

Sample Preparation

Friction experiments were conducted at room temperature on serpentinite rings with bare surfaces as well as on $\sim$1 mm layers of powdered serpentinite sandwiched between quartzite rings. Two sample geometries have been used for the friction experiments in this study (Figure 2). The majority of the bare surface experiments were conducted using the jacketed sample geometry shown in Figure 2a; one experiment was conducted on bare surfaces of GC serpentinite using the unjacketed sample geometry in Figure 2b. All of the powdered serpentinite experiments were conducted using the jacketed sample geometry shown in Figure 2a with a layer of simulated gouge between the sample rings.

Both serpentinite and quartzite rings were initially ground flat on a surface grinder, then roughened by hand on a glass plate with 24-grit alumina abrasive. Because the serpentinite and quartzite we used are nearly impermeable to gas, a 1.1 mm hole was drilled through the upper sample rings for the jacketed experiments in order to vent the sliding surface to the atmosphere in case of jacket leakage. In the experiment on VM2 serpentinite, the material in the small white

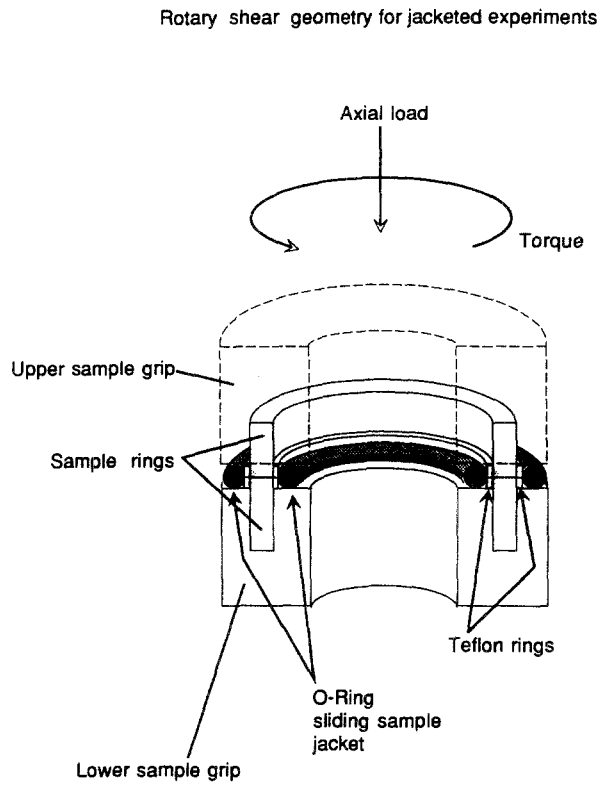

Figure 2(a)

veins that intersected the sliding surface was removed by hand-picking the fibers under a binocular microscope prior to assembling the experiment.

We conducted friction experiments on simulated gouge samples of both GC and T91NI6 serpentinites. The gouges were prepared by crushing the serpentinites in a ball mill and passing the resulting powder through an 88 μm sieve. The simulated gouges were then stored in sealed glass jars at room humidity.

All of the bare-surface experiments were assembled at room humidity and the surfaces of the jacketed sample rings were moistened with distilled water prior to assembling an experiment. We did not add water to the unjacketed sample. Humidity varies greatly with the season and is higher in summer than in winter. Early experiments on simulated gouge (prior to January 25, 1992) were assembled at room humidity with the surface of one quartzite ring dampened with distilled water. Later gouge experiments were assembled in a glove bag at room temperature with the relative humidity controlled to nearly 100% by bubbling air through water at the intake to the glove bag; the surface of one sample ring was dampened with distilled water.

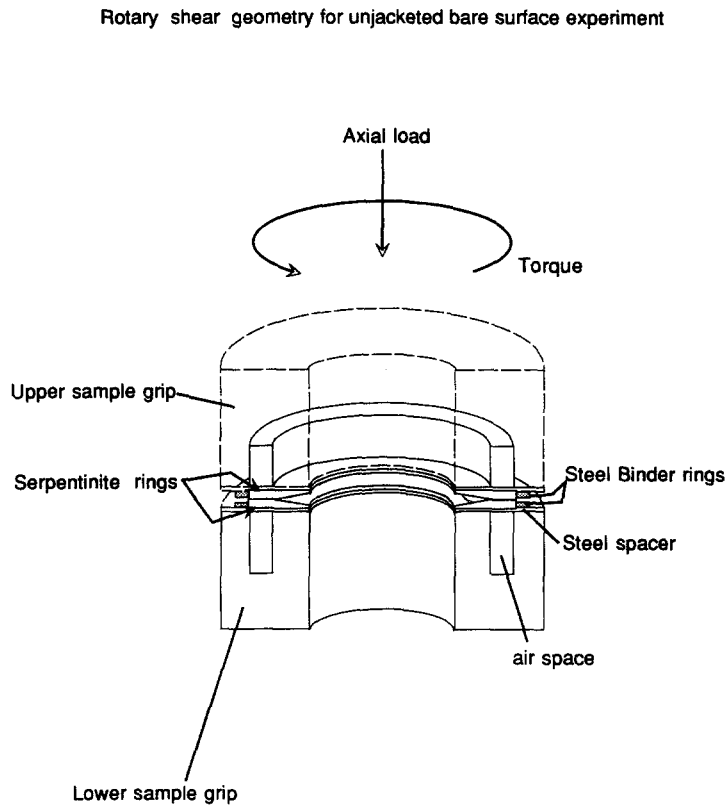

Figure 2(b)

Figure 2

Schematic cut-away view of the rotary-shear sample geometries used in this study. The outer diameter of the sample rings is 54 mm. (a) Sample geometry used for jacketed experiments. The O-rings provide a sliding seal, while the Teflon rings distribute the confining pressure along the sides of the sample and allow for slip between the O-rings and the sample rings. (b) Unjacketed sample geometry used in the experiment with no confining pressure. The inner beveling of the sample rings and outer steel binder rings help the sliding rings maintain integrity.

Results and Interpretations

Frictional Strength

The relationship between shear and normal stresses indicates whether our samples are undergoing frictional sliding or plastic yielding. The steady-state shear strength of both of the antigorite serpentinites displays a nearly linear dependence on normal stress (Figure 3). The slopes of these lines yield a coefficient of friction between 0.5 and 0.6, indicating that antigorite serpentinite is not a particularly weak rock. At 0.01 μm/s and normal stresses greater than 100 MPa, there is an

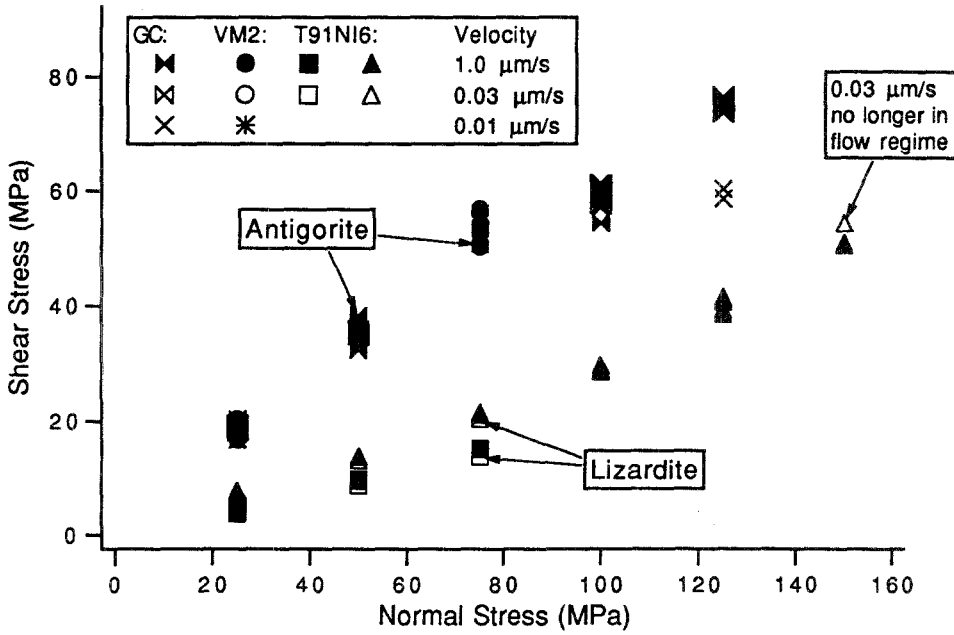

Figure 3
Steady-state shear resistance to sliding as a function of normal stress for the serpentinites in this study.

apparent curvature of the yield envelope for GC serpentinite indicating a possible change in mechanical behavior from frictional sliding to plastic flow. The steady-state shear strength of lizardite serpentinite gouge displays linear dependence on normal stress up to 150 MPa normal stress for velocities of 1.0 and 0.032 μm/s (Figure 3). The slope of the yield envelope ($\sim$0.2 to 0.3) of lizardite serpentinite is considerably less than that of antigorite serpentinite. The linear form of the envelope indicates that the low frictional strength of the lizardite serpentinite is not due to plastic flow of serpentinite. For the remainder of the paper, we define the coefficient of friction as the ratio of shear to normal stress, rather than the slopes of the yield envelopes shown in these figures.

The coefficient of friction of antigorite serpentinite ranges between 0.5 and 0.85 in bare-surface experiments conducted with normal stresses between 25 and 125 MPa, and between 0.5 and 0.75 for gouge experiments conducted at 25 MPa normal stress. These values are similar to the value of 0.77 reported by DENGO and LOGAN (1981) on bare surfaces of an antigorite serpentinite of composition similar to those used in this study. However, we find that the coefficient of friction for lizardite serpentinite gouge ranges between 0.15 and 0.35; DENGO and LOGAN (1981) reported a value of 0.56 for a serpentinite consisting of 70% serpentine (mostly lizardite), 19% oxides, 11% enstatite, and minor amounts of olivine. The

higher coefficient of friction reported by Dengo and Logan, relative to the lizardite samples in this study, may result from the enstatite and oxides in their sample.

Effects of Water

The frictional behavior of serpentinite is sensitive to the amount of water present in the samples during assembly. Figure 4 shows the effect of varying the water content in antigorite serpentinite gouge samples. The terms "dry," "damp," and "wet" are relative: the "dry" experiment was assempled at room humidity (January) with no water added to the sample, the "damp" experiment was assembled at room humidity (August) with distilled water added to one forcing block, and the "wet" experiment was assembled in a humid glove bag with distilled water added to one forcing block.

Increasing the relative wetness of an antigorite gouge sample produces two effects: it decreases the frictional strength of the sample and it increases the velocity at which the transition between velocity strengthening (at low velocities) and velocity weakening (at high velocities) occurs. In Figure 4, velocity strengthening is indicated by a positive slope to the data, while velocity weakening may be indicated by either a negative slope or by stick-slip behavior. The transition velocity is around 0.10 μm/s in the "wet" experiment and around 0.032 μm/s in the "damp" experment. The "dry" experiment exhibited stick-slip motion over the entire velocity range tested,

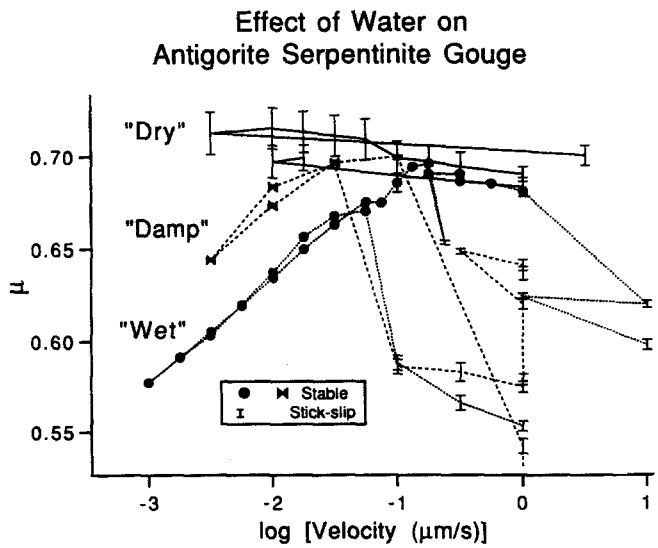

Figure 4
Effect of water on the frictional strength of antigorite serpentinite gouge. Solid symbols indicate stable sliding, and bars indicate the range of stress drops during stick-slip sliding; the lines connecting the symbols indicate the sequence of velocities sampled in an experiment.

indicating a transition velocity lower than 0.0032 μm/s. In the experiment on bare surfaces of unjacketed antigorite, stick-slip sliding observed at low velocities is indicative of velocity-weakening behavior. This experiment was assembled at room humidity (late November) with no water added to the sample surface. We believe that the velocity weakening observed at low velocities is due to the absence of excess water on the sliding surfaces, resulting in a transition velocity lower than those sampled during the experiment.

Velocity-step Tests

Frictional velocity dependence:

At high velocities, state-variable behavior is apparent in the transient direct effect (as a peak in friction following a velocity increase, or as a transient drop in friction following a velocity decrease), and the subsequent evolution to the new steady-state level (evolution effect; Figure 5). At high velocities, sliding was stable in the experiments on bare surfaces of antigorite serpentinite and in the experiments on lizardite gouge, and the steady-state friction levels are readily determined. In the experiments on gouge layers of antigorite serpentinite, sliding occurred by stick-slip motion at high velocities and steady-state was not achieved. The velocity dependence of the serpentinites reported here was determined from the stable sliding portions of the experiments only; we presume that stick-slip indicates velocity weakening of unknown magnitude.

At low velocities, all the serpentinites typically undergo stable sliding and display large direct effects with little or no evolution effects. VM2 shows a slight evolution effect at low velocities, indicating an incomplete transition to flow behavior, possibly caused by contamination of the sliding surface with magnesite. The oscillations observed in the VM2 experiments at all velocities are similar to those observed by WEEKS and TULLIS (1985) in experiments conducted on dolomite, and are another indication of possible contamination of the sliding surface by magnesite.

The steady-state velocity dependence of bare surface antigorite serpentinite is summarized in Figures 6a and 6b. At all normal stresses tested, both antigorite serpentinites exhibit velocity-strengthening behavior at low velocities, with a transition to velocity-weakening behavior at higher velocities. The transition in the GC serpentinite occurs between 0.032 to 0.100 μm/s, and it occurs in the VM2 samples between 0.010 and 0.032 μm/s. This transition in velocity dependence is similar to that found in halite which has been correlated to a change in dominant deformation mechanisms (CHESTER and LOGAN, 1990). At the highest velocities tested, GC serpentinite continues to exhibit velocity weakening and VM2 serpentinite displays velocity strengthening. At high velocities, VM2 shows short-term velocity weakening with long-term velocity strengthening (Figure 5b). This long-term velocity-strengthening behavior is similar to that observed in dolomite marble

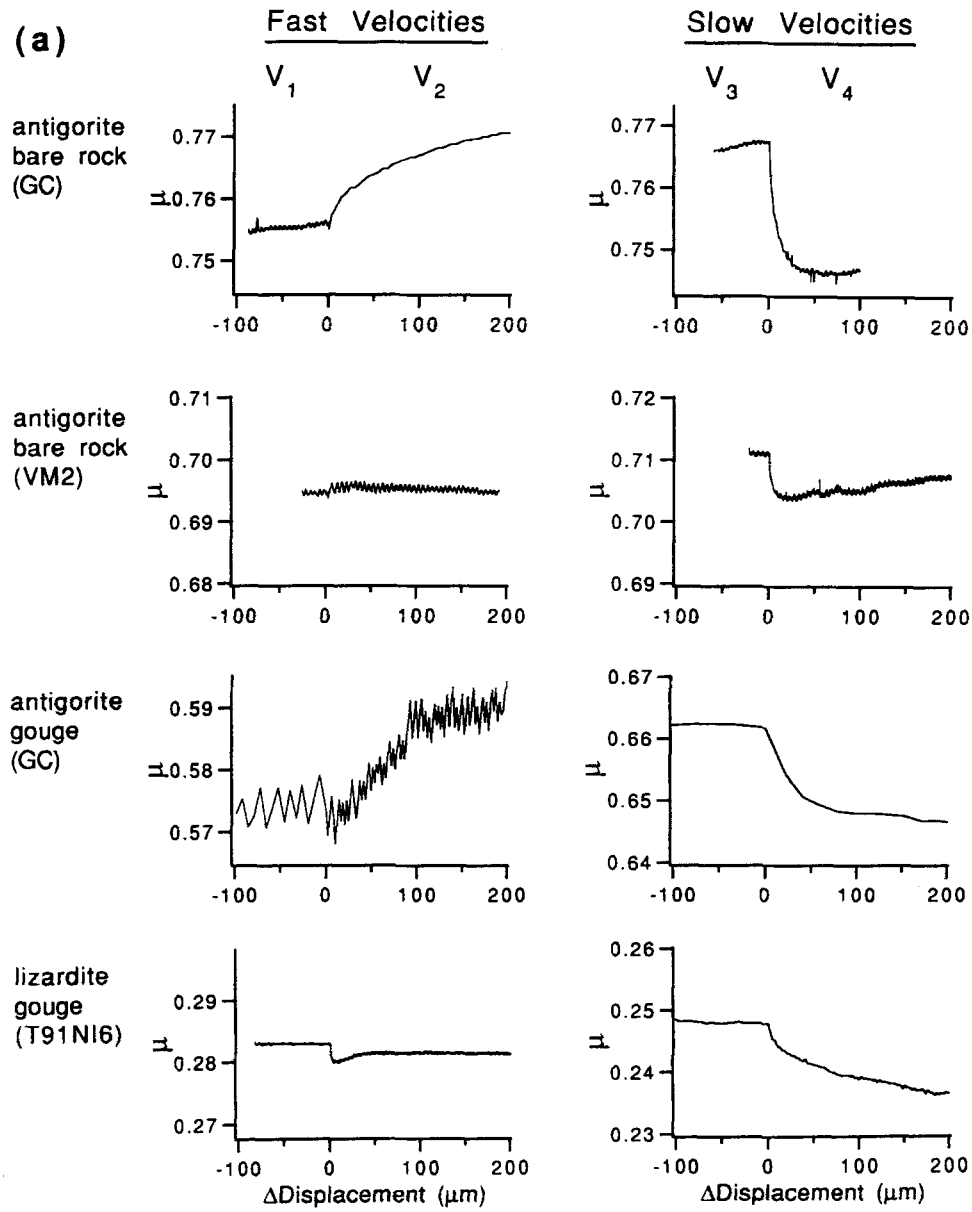

Figure 5(a)

by WEEKS and TULLIS (1985), indicating that the magnesite in the VM2 serpentinite may make a significant contribution to the frictional behavior at high velocities. In an additional experiment on VM2 serpentinite, the magnesite and serpentine fibers were not removed from the small veins intersecting the sliding surface (see **Sample Preparation** above); the velocity dependence of this sample

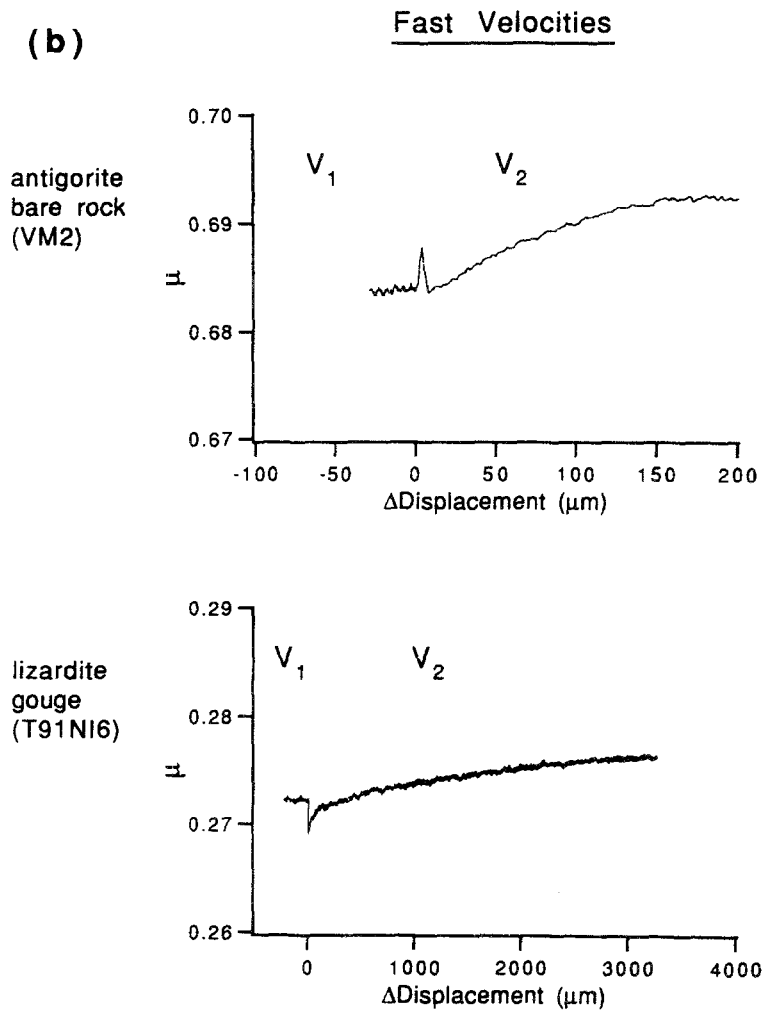

Figure 5(b)

Figure 5

Frictional response to a step change in loading velocity as a function of displacement for the different serpentinites at room temperature and 25 MPa normal stress. In all of the figures, the displacement (horizontal) scale is set such that the change in loading velocity occurs at zero displacement. (a) Comparison between high velocity (state variable) and low velocity (flow) behavior of the different types of experiments. The velocity steps shown all involve a step from a higher velocity to a lower velocity. Velocities in $\mu m\ s^{-1}$ are: GC bare rock ($V_1 = 1.0$, $V_2 = 0.32$, $V_3 = 0.010$, $V_4 = 0.003$); VM2 bare rock ($V_1 = 1.0$, $V_2 = 0.32$, $V_3 = 0.010$, $V_4 = 0.003$); GC gouge ($V_1 = 1.0$, $V_2 = 0.32$, $V_3 = 0.018$, $V_4 = 0.010$); T91NI6 gouge ($V_1 = 1.0$, $V_2 = 0.32$, $V_3 = 0.018$, $V_4 = 0.010$). (b) VM2 and T91NI6 gouge showing high velocity behavior over long displacements. VM2 responds to a step increase in velocity ($V_1 = 1.0$, $V_2 = 10.0$) with short-term velocity weakening and long-term strengthening with displacement, in contrast to observations at lower velocities or the other serpentinites. In contrast to the behavior of antigorite, lizardite serpentinite gouge ($V_1 = 3.2$, $V_2 = 1.0$) shows short-term velocity strengthening and long-term velocity weakening (note scale-change).

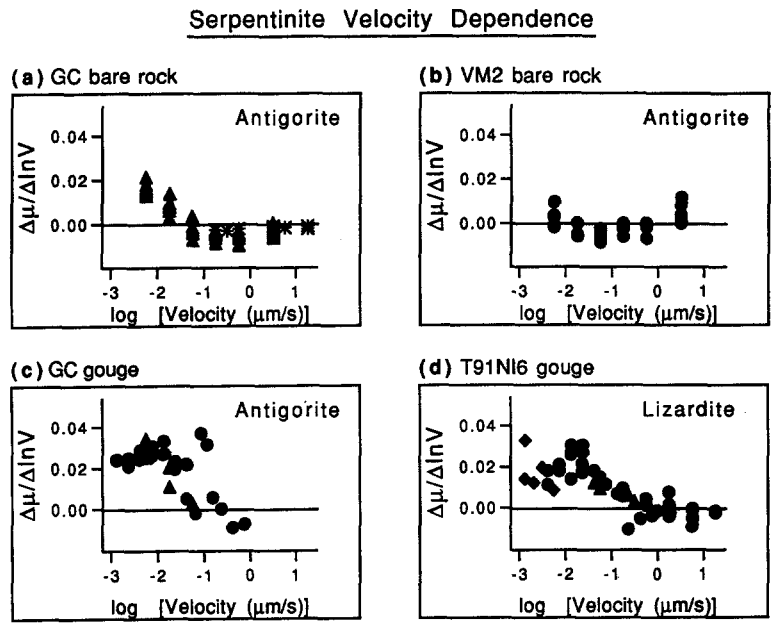

Figure 6

Steady-state velocity dependence at 25 MPa normal stress. Each point is plotted at the geometric mean of the velocities before and after a given velocity step. All three serpentinites show a transition from velocity strengthening at low velocities to velocity weakening or velocity neutral at high velocities. (a) GC bare surfaces. X's in the 25 MPa inset show the results from the unjacketed experiment. For velocity dependence at higher normal stresses, see REINEN *et al.* (1991). (b) VM2 bare surfaces. (c) GC gouge; only stable sliding velocity steps are shown. Triangles (fr101) and circles (fr105) are results from different experiments. (d) T91NI6 gouge; only stable sliding velocity steps are shown. Diamonds (fr109), circles (fr114) and triangles (fr117) are results from different experiments.

strongly resembles that of calcite and dolomite, with the magnitude of the velocity-weakening behavior increasing with decreasing velocity (see REINEN, 1993; WEEKS, 1993). In contrast to experiments on jacketed GC serpentinite with bare surfaces, the unjacketed sample of GC serpentinite was velocity weakening over the range of velocities tested.

The steady-state velocity dependence of antigorite serpentinite gouge is shown in Figure 6c. The velocity dependence of the gouge undergoes a transition between 0.032 and 0.32 μm/s similar to that observed in the bare surface experiments, from velocity strengthening at low velocities to velocity weakening at high velocities. At high velocities, few data points are shown due to the occurence of stick-slip sliding of the gouge; only immediately following sliding at low velocities did the gouge layers undergo stable sliding at these higher velocities. The stick-slip sliding is another indication of the velocity-weakening nature of antigorite serpentinite gouge at high velocities.

The velocity dependence of lizardite serpentinite gouge is shown in Figure 6d. The transition in velocity dependence between 0.32 and 1.0 μm/s is similar to that

observed in antigorite serpentinite experiments. Lizardite serpentinite exhibits the two-mechanism behavior previously described for antigorite serpentinite. At high velocities, antigorite serpentinite is velocity weakening, both over the short term (see Figure 5a) and with continued displacement. In contrast, lizardite serpentinite shows short-term velocity strengthening at high velocities, with up to 6000 μm displacement required for a complete evolution to velocity weakening or velocity-independent friction (Figure 5b). At low velocities, both antigorite and lizardite serpentinites are strongly velocity strengthening.

Velocity-step test simulations:

The transition in velocity dependence of the serpentinites in this study is an indication of two mechanisms accommodating deformation in our experiments. We have previously modeled velocity-step data from experiments on bare surfaces of antigorite serpentinite using the two-mechanism model (REINEN, 1992a,c). We have extended this modeling to include results from experiments conducted on gouge layers of antigorite serpentinite and lizardite serpentinite.

The response of bare surfaces of antigorite serpentinite to a series of step-changes in loading velocity is shown in Figure 7. We have modeled this data using the two-mechanism constitutive model; the parameters used for this fit are listed in Table 2. The simulation matches the observed state-variable behavior well at high velocities, with a small direct effect and a much larger evolution effect. At low velocities, the simulation matches the observed flow behavior with a very large

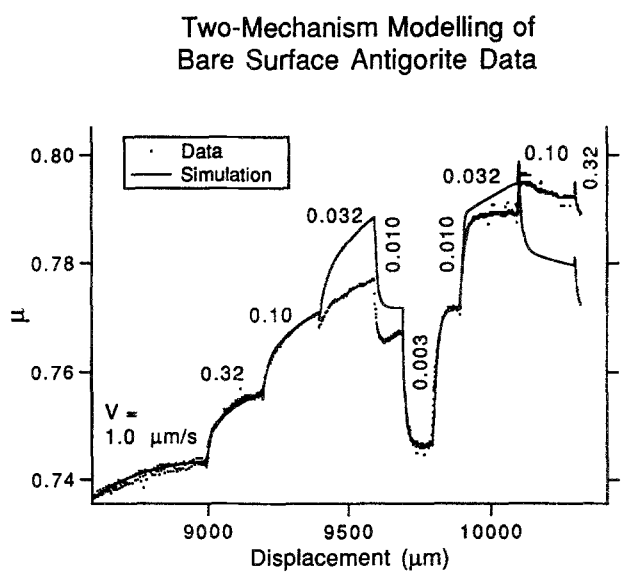

Figure 7

Friction versus displacement for a series of velocity steps in an experiment conducted on bare surfaces of antigorite serpentinite. Dots are experimental data; the line is a simulation using the two-mechanism constitutive model.

Table 2

Constitutive parameters used in forward modeling of serpentinite velocity-step data. Subscripts F and SV refer to flow mechanism and state-variable mechanism parameters

Material	$\mathbf{a}_F$	μ_F^*	$\mathbf{a}_{SV}$	μ_{SV}^*	$\mathbf{b}_1$	D_{c1}	$\mathbf{b}_2$	D_{c2}
GC bare surfaces	0.0220	0.7450	0.00150	0.6453	0.0060	15.0	0.00900	190.0
GC gouge	0.0296	0.7820	0.00780	0.6328	0.00340	4.62	0.01800	118.79
T91NI6 gouge	0.0230	0.3390	0.00343	0.2835	0.00156	14.0	0.00068	590.0

direct effect and no evolution effect; the rounded transition with displacement between the two steady-state levels is caused by machine compliance. At transitional velocities the fit to the data is not as close; the transition between the state-variable and flow mechanism takes place over shorter time (or displacement) in the model than in the data. However, the form of the frictional behavior of the data and the model is quite similar at these intermediate velocities.

The response of antigorite serpentinite gouge to a series of step changes in loading velocity is shown in Figure 8 along with a simulation using the two-mechanism model. Table 2 contains a list of parameters for this fit. For velocities ≥ 0.10 μm/s, the velocity-weakening nature of the state-variable behavior results in stick-slip sliding. During the stick-slip sliding portion of this experiment, an evolution effect is still observed (seen in Figure 8 by the increase in friction following the velocity step from 0.32 to 0.10 μm/s). With the decrease in loading velocity to 0.056 μm/s, a transition in behavior occurs involving an increase in frictional strength and a change to stable sliding. Subsequent velocity steps show velocity strengthening; for velocities ≤ 0.018 μm/s, no evolution effect is apparent. The model is not presently equipped to handle stick-slip sliding, therefore the simulation initiates during the rise in stress near 6500 μm displacement. As a result, the state-variable model parameters are not constrained by these data. In Figure 8, the best forward model is compared with a simulation generated using the parameters determined for the bare surface data shown in Figure 7, indicating that the model parameter $\mathbf{a}_F$ for the gouge experiment is slightly greater than $\mathbf{a}_F$ for the bare surface experiment (Table 2). At low velocities, the fit between the simulations and the data is not as good as for the bare surface experiment. The misfit might be due to either a decrease in effective stiffness of the gouge layer relative to the bare surfaces or to shearing within the gouge layer. An incorrect choice for effective stiffness would result in an incorrect loading slope immediately following a change in velocity, which is not observed. Distributed deformation within the gouge layer is not accounted for in our model. We assume that slip occurs on a discrete surface,

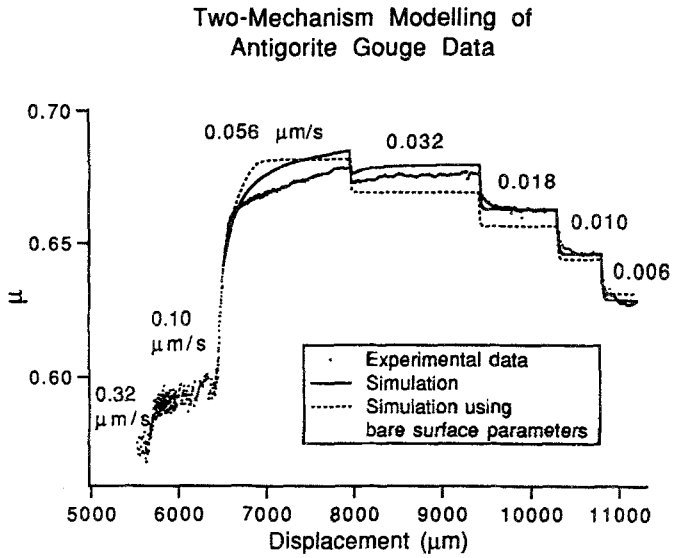

Figure 8

Friction versus displacement for a series of velocity steps in an experiment conducted on antigorite serpentinite gouge. Dots are experimental data, the lines are simulations using the two-mechanism constitutive model. The solid line is a simulation from parameters chosen to match these data; the dashed line is a simulation using the parameters that fit the velocity steps shown in Figure 7. The transition to stable sliding does not coincide with a velocity step; the sample had been sliding for about 200 μm when sliding stabilized. The simulations start during the stress rise that accompanies the transition to stable sliding.

whereas slip may occur throughout the gouge layer. The misfit between the experimental data and the simulation at these low velocities is probably a result of flow within the gouge layer. This contention is supported by the better fit of the model to low-velocity data from bare surfaces than from gouge layers.

The response of a gouge layer of lizardite serpentinite to a series of step-changes in loading velocity is shown in Figure 9 along with a simulation using the two-mechanism constitutive model; the parameters used for this fit are listed in Table 2. In this experiment, the velocity dependence of the state-variable mechanism is very small with short-term velocity strengthening, resulting in stable sliding over the entire range of velocities tested. The simulation matches the state-variable behavior of the data well at high velocities. While the predicted stress levels match the data at low velocities, the experimental data show a much more rounded transient response than predicted by the model. As in the antigorite serpentinite gouge experiment, the misfit between the experimental data and the simulation at these low velocities may result from flow within the gouge layer that is not included in the model.

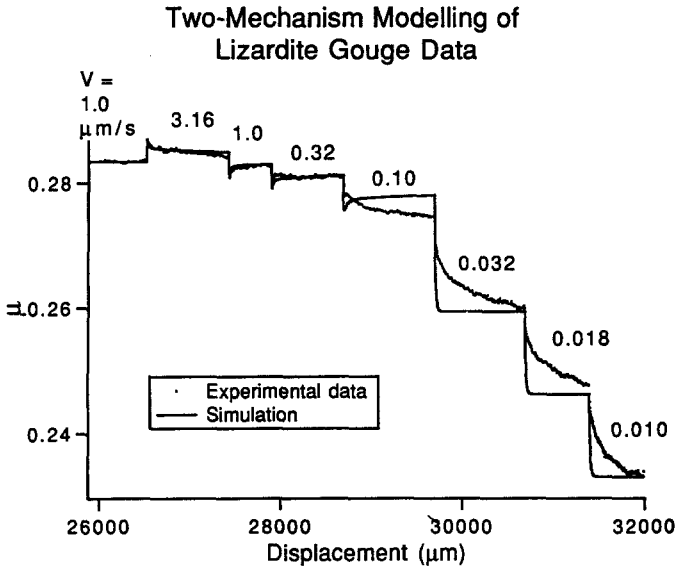

Figure 9
Friction versus displacement for a series of velocity steps in an experiment conducted on lizardite serpentinite gouge. Dots are experimental data; the line is a simulation using the two-mechanism constitutive model.

Timed-hold Tests

We conducted timed-hold tests on gouge layers of both antigorite and lizardite serpentinite in order to test whether two mechanisms contribute to the frictional time dependence. All of the timed-hold tests in this study were conducted on layers of serpentinite gouge, not on bare surfaces. The response of serpentine to hold tests does reflect two-mechanism behavior, with the different responses dependent on both the initial velocity prior to the hold and upon the length of hold time.

Two-mechanism behavior in the serpentinite experiments is reflected in the response of the serpentinites to reloading following a hold (Figure 10). For holds initiated at sliding velocities below the transition velocity ($V_{trans} \cong 0.1$ μm/s for antigorite and $\cong 1.0$ μm/s for lizardite), the behavior of both antigorite and lizardite

Figure 10
Examples of timed-hold tests on antigorite and lizardite gouge for both short and long holds. (a) Reloading curve of antigorite gouge from a hold initiated from a velocity (0.006 μm/s) below V_{trans}, illustrating the simple reloading shape of both serpentinites from holds occurring entirely in the flow-dominated regime. (b) Lizardite gouge. Load point velocity was 3.16 μm s^{-1} which is above V_{trans} for this material. (c) Antigorite (GC) gouge. Load point velocity was 0.316 μm s^{-1} which is above V_{trans} for this material. Sliding was by stick-slip motion in the antigorite gouge layer, until stick-slip was suppressed by the long holds.

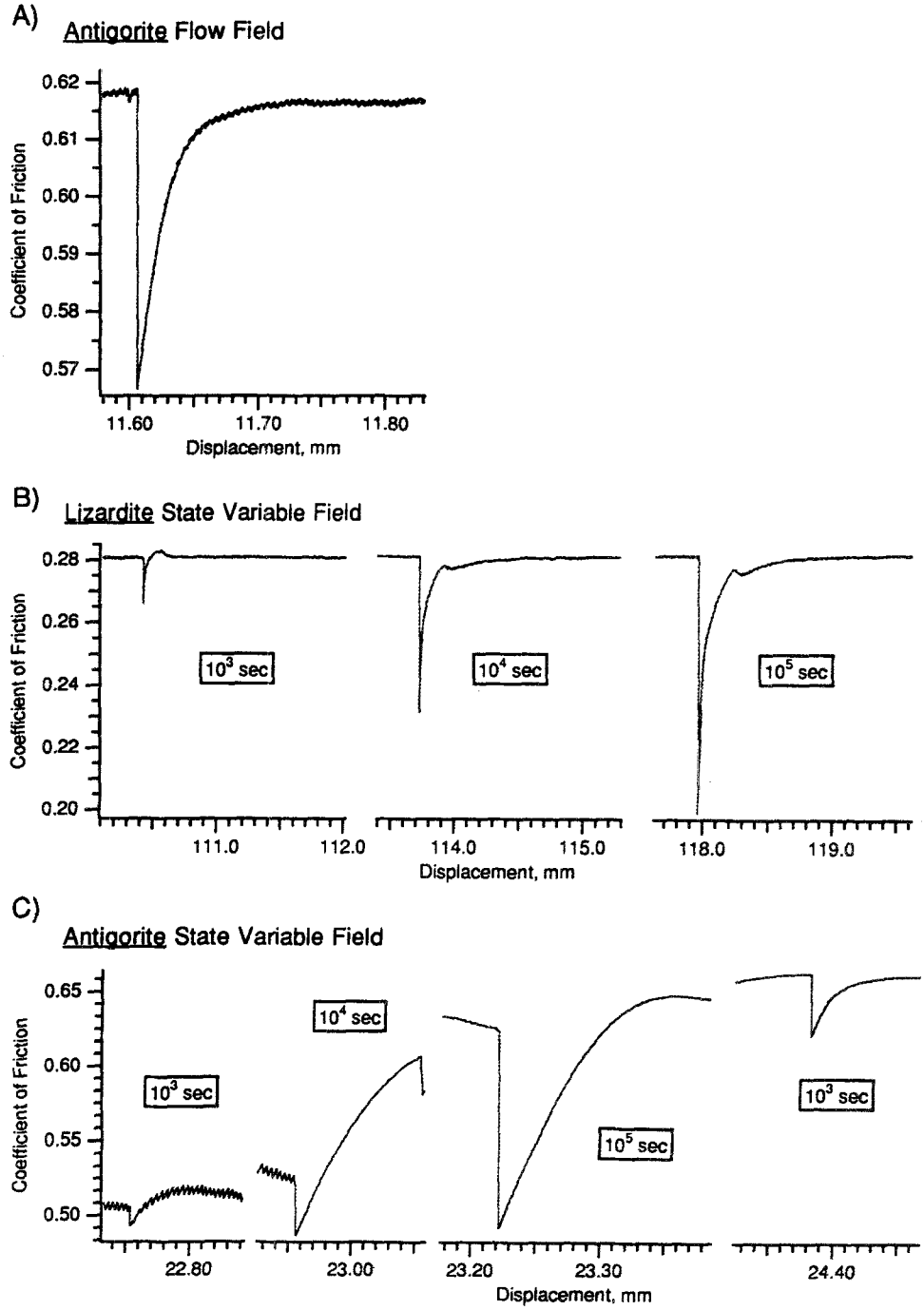
A)
Antigorite Flow Field
Coefficient of Friction
0.62
0.61
0.60
0.59
0.58
0.57
11.60
11.70
11.80
Displacement, mm
B)
Lizardite State Variable Field
Coefficient of Friction
0.28
0.26
0.24
0.22
0.20
10^3 sec
10^4 sec
10^5 sec
111.0
112.0
114.0
115.0
118.0
119.0
Displacement, mm
C)
Antigorite State Variable Field
Coefficient of Friction
0.65
0.60
0.55
0.50
10^3 sec
10^4 sec
10^5 sec
10^3 sec
22.80
23.00
23.20
23.30
24.40
Displacement, mm

gouge is the same as one another and is very simple. It consists merely of a gradual return climb to the steady-state level (Figure 10a).

For holds initiated from velocities higher than V_{trans} the reloading responses of the serpentinites is more complex, with the response of the antigorite gouge complicated by stick-slip sliding at high velocities. For this reason, we discuss the simpler response of lizardite gouge to holds before discussing antigorite gouge. Lizardite gouge exhibits stable sliding at high velocities, and upon reloading after short hold times the coefficient of friciton rises over a transient peak followed by a return to $\mu_{steady\text{-}state}$ (Figure 10b, 10^3 sec hold). This transient peak is similar to that observed for quartzite and granite (e.g., DIETERICH, 1972 and 1979), and is evidence of the evolution effect active in the lizardite gouge at high velocities. Following longer hold times, there is a local maximum similar to the peak expected after a hold, but it is not at the maximum friction level. The small bump on reloading after the longer holds on lizardite, while not as high as the steady-state stress, presumably represents the time-dependence of the state-variable mechanism.

For holds on antigorite gouge initiated from velocities higher than V_{trans}, friction traces upon reloading from a hold show two distinct forms, depending on the length of the hold and the history of previous sliding. Sliding at high velocities on antigorite gouge occurs by stick slip regardless of previous history, provided that sliding continues over a sufficiently long distance. Reloading from short holds initiated during stick-slip sliding involves an unusual increase in resistance composed of stick-slip events in which the envelope of the stick-slip events follows the usual peak and steady-state level behavior (first 10^3 sec hold in Figure 10c). Reloading from intermediate-length holds following stick-slip sliding reveals no stick slip during the loading and the friction increases to a considerably higher level before an eventual stick slip event (3.2×10^4 sec hold in Figure 10c). After even longer holds, the behavior is similar except that the friction level reached is even higher and sliding is initially stable (10^5 sec hold in Figure 10c). A subsequent short hold initiated after small displacement remained strong during the relaxation and was followed by stable sliding. The reload following the short hold climbed back to the same high friction level that existed before the hold and continued to slide stably (final 10^3 sec hold in Figure 10c). The two 10^3 sec holds in Figure 10c conducted at different times during this experiment differ significantly and depend on previous slip history.

The change in the form of reloading from timed holds is consistent with the two-mechanism model. In our experiments, we set the loading velocity to zero during the hold, but the velocity at the sliding surface is not zero due to relaxation of the spring between the loadpoint and the surface. If the loading velocity and the slip velocity are not equal, the shear stress changes according to:

$$\frac{d\mu}{dt} = k(V_0 - V) \tag{6}$$

in which the change in fricitonal stress with time is proportional to the difference between the loading velocity V_0 and the sliding velocity V through the spring constant k. During the hold portion of the test, V_0 is zero, so that $d\mu/dt = -kV$.

During a hold, the sliding velocity approaches zero, allowing us to sample ever-decreasing velocities. Holds initiating from velocities less than V_{trans} should only sample flow-mechanism behavior which lacks a time-dependent term. Consequently such hold tests should not exhibit a transient peak in the frictional level upon reloading and, indeed, we do not observe a transient peak in our experiments under these conditions. Holds initiated at higher velocities start in the state-variable-dominated regime. During short holds, the serpentinite is in the state-variable-dominated regime and should display a transient peak frictional level upon reloading, indicative of the evolution effect of the state-variable mechanism; this is observed in our experiments. During long holds initiated from high velocities, the serpentinite begins in the state-variable-dominated regime but eventually moves into the flow-dominated regime as the velocity decreases. Reloading from these long holds should be influenced by the flow-dominated regime. This is expressed in antigorite by the stable sliding following long holds, as well as the metastable high stress and stable sliding in subsequent shorter holds (Figure 10c, second 10^3 sec hold). We presume that following long holds, the transient peak in lizardite is caused by the evolution effect and that the higher steady-state friction level reflects the flow mechanism, but we do not understand this behavior in detail.

Strengthening during holds:

The peak friction levels of the antigorite serpentinite gouge for timed holds conducted during two experiments and at three loading velocities are shown as a function of hold time in Figures 11a and 11b. For a loading velocity of 0.32 μm/s, there are two peak friction levels for any given hold time (Figure 11a). In the antigorite serpentinite experiment fr101, after sufficiently long holds the peak friction level saturates and subsequent shorter holds do not revert back to weaker, stick-slip sliding as expected; they remain stable and the peak friciton level is almost invariant with hold time. In experiment fr105, the peak friction level rises after long holds, but may not have reached saturation; a subsequent 10^2 sec hold does revert back to the weaker stick-slip sliding mode. One set of timed holds for experiment fr105 followed sliding at much lower velocities (solid diamonds connected by solid line) began and remained at the strong and stable peak friction level. Figure 11b shows peak friction levels for loading velocities of 0.006 and 3.16 μm/s. The holds at the lower loading velocity remain stable for the range of hold times tested and the peak friction levels are single valued; the holds at the higher loading velocity achieve an apparent peak friction saturation while continuing to stick slip during reloading.

The peak friction levels of the lizardite serpentinite gouge for timed holds conducted during two experiments and at two loading velocities are shown in

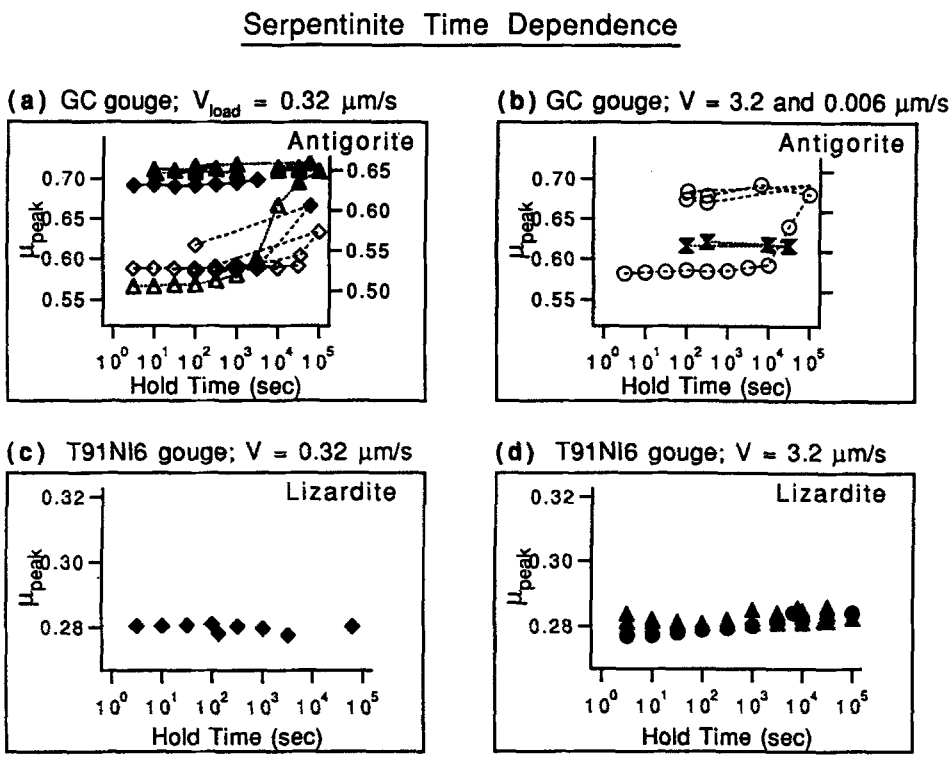

Figure 11
Peak friction of serpentinite gouge versus hold time. (a) GC gouge with $V_{load} = 0.32$ μm/s, illustrating the two-mechanism behavior of antigorite serpentinite. Open symbols indicate holds for which the serpentinite was stick-slipping before and after the holds; solid symbols indicate holds for which the serpentinite slid stably. Lines connect the data points in the order in which the hold tests were performed. Triangles (fr101) are plotted relative to the right axis; diamonds (fr105) relative to the left axis. (b) GC gouge with $V_{load} = 3.2$ μm/s (circles) and 0.006 μm/s (hour glasses) from experiment fr105. (c) T91NI6 gouge with $V_{load} = 0.32$ μm/s. (d) T91NI6 gouge with $V_{load} = 3.2$ μm/s ($> V_{trans}$ for lizardite). Circles and triangles show two different hold series conducted during one experiment (fr114).

Figures 11c and 11d. For loading velocities of both 0.32 and 3.2 μm/s, the peak friction levels remain essentially invariant with hold time.

The double-valued nature of the peak friction levels observed in the antigorite serpentinite gouge at velocities ≥ 0.32 μm/s in Figure 11 reflects the double-valued steady-state friction levels for loading velocities greater than the transitional velocity (Figure 1a). Because the loading velocity during reloading from a hold is much higher than the current slip velocity, reloading takes place along a constant-state line in Figure 1a. This brings the trajectory up along the upper branch of the steady-state curve. As in velocity-step tests, the transition between mechanisms in the experimental data is sluggish compared to model predictions, allowing a large number of hold tests to occur completely on the upper branch. If the loading

velocity is below the transition velocity, all deformation takes place in the flow mechanism, and only one possible response is predicted by the model. This is in fact what we observe in hold tests at low loading velocity (0.006 μm/s in Figure 11b).

When the same type of test is performed on lizardite, which has a velocity-strengthening response in the state-variable field, the results are single-valued over the entire range of hold times tested (Figure 11). As seen in Figure 1b, when the state-variable component has a velocity-strengthening steady-state response, combined steady-state exists at all velocities. This predicts the single-valued peak friction results that are observed in our experiments.

Behavior during relaxations:

That two mechanisms accommodate deformation of serpentinite is evident in the frictional relaxations during timed-hold tests on both antigorite and lizardite serpentinite gouges. When relaxations performed on serpentine are plotted as frictional strength versus log of time, the change in mechanism at low velocity is seen clearly. The shapes of the relaxations during $10^{4.5}$ sec (8.8 hours) holds in the antigorite serpentinite are shown in Figure 12a. In this figure, holds initiating from three different loading velocities are shown. For two of these velocities, 0.32 and 3.2 μm/s, sliding occurred by stick-slip motion prior to the timed holds. The relaxations for holds starting at these higher velocities show an initial shallow slope followed by a large increase in slope at long times. A similar marked increase in slope has been observed for quartz gouge under hydrothermal conditions and has been correlated to a change in deformation mechanism by microstructural observations (CHESTER and HIGGS, 1992).

The shapes of the relaxation curves during $10^{4.5}$ sec holds in the lizardite serpentinite gouge have been examined in two experiments and two velocities (Figure 12b). Prior to the holds, sliding was stable in experiment fr114, whereas sliding was unstable in experiment fr109. Where sliding was stable prior to the hold, the initial frictional decrease upon initiation of the hold reflects the state-variable direct effect, and the subsequent deviation from this initial line (upward concavity) reflects strengthening with continued evolution of the state variables (the evolution effect). Where sliding was by stick-slip motion prior to the hold, the system was not at steady-state and the relaxation does not show a direct and evolution effect at short times (compare with Figure 12c). However for both cases in Figure 12b, the initial form of the serpentinite relaxations changes to a large increase in slope at longer times, indicating the influence of the flow mechanism at lower sliding velocities.

For holds initiated from loading velocities less than V_{trans}, only the flow mechanism of the two-mechanism model should be sampled. Our experiments show that neither antigorite nor lizardite serpentinite gouge display state-variable behavior in relaxations starting from velocities less than V_{trans} (Figures 11 and 12a).

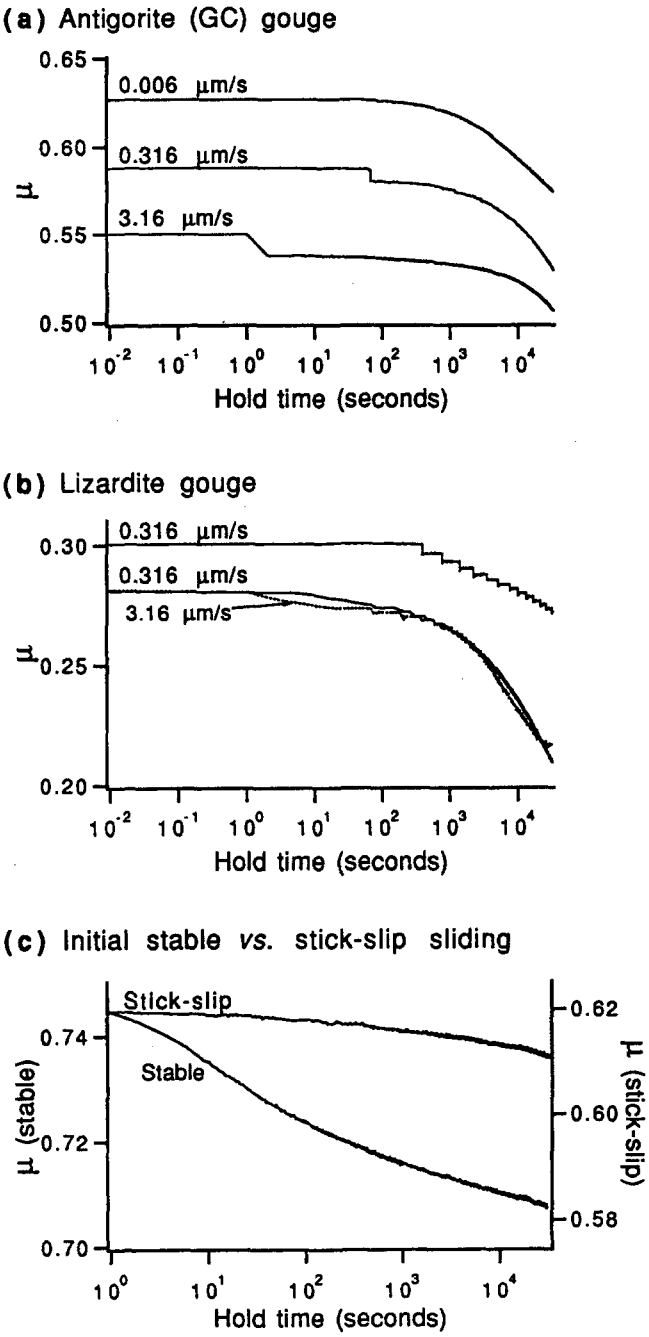
(a) Antigorite (GC) gouge
0.65
0.60
0.55
0.50
μ
0.006 μm/s
0.316 μm/s
3.16 μm/s
10^-2 10^-1 10^0 10^1 10^2 10^3 10^4
Hold time (seconds)
(b) Lizardite gouge
0.30
0.25
0.20
μ
0.316 μm/s
0.316 μm/s
3.16 μm/s
10^-2 10^-1 10^0 10^1 10^2 10^3 10^4
Hold time (seconds)
(c) Initial stable vs. stick-slip sliding
Stick-slip
Stable
0.74
0.72
0.70
μ (stable)
0.62
0.60
0.58
μ (stick-slip)
10^0 10^1 10^2 10^3 10^4
Hold time (seconds)

The parameter $\mathbf{a}_F$ can be directly determined from the low-velocity portions of the stress relaxation data. We model the low-velocity relaxations with the flow constitutive law (equation (2)) interacting with the spring equation (equation (6)). The derivative of the flow constitutive law with respect to time is

$$\frac{d\mu}{dt} = \mathbf{a}_F \frac{d \ln V}{dt} = \frac{\mathbf{a}_F}{V}\frac{dV}{dt}. \tag{7}$$

During a relaxation, the loadpoint velocity V_0 is zero. Setting equation (7) equal to equation (6) yields the differential equation

$$\frac{dV}{dt} = -\frac{k}{\mathbf{a}_F} V^2 \tag{8}$$

with a solution

$$V = \frac{\mathbf{a}_F/k}{\beta + t}. \tag{9}$$

If we assume that $\partial\mu/\partial t = 0$ (see equation (6)) before the hold, then at the start of the hold ($t = 0$) V is the sliding velocity ($V = V_{\text{init}}$) and

$$\beta = \frac{\mathbf{a}_F}{kV_{\text{init}}}. \tag{10a}$$

The solution to equation (8) is then

$$V = \frac{\mathbf{a}_F/k}{\dfrac{\mathbf{a}_F}{kV_{\text{init}}} + t} = \frac{V_{\text{init}}}{1 + \left(\dfrac{kV_{\text{init}}}{\mathbf{a}_F}\right)t}. \tag{10b}$$

During the relaxation, V starts at V_{init} and decreases with increasing t. Using this solution in equation (2) yields

$$\mu = \mu_F^* + \mathbf{a}_F \ln\left(\frac{\mathbf{a}_F}{kV_F^*}\right) - \mathbf{a}_F \ln(\beta + t). \tag{11}$$

Figure 12

Examples of frictional relaxations during timed-hold tests. (a) Relaxations during $10^{4.5}$ sec holds on GC serpentinite gouge from three different initial loading velocities. During the holds, the 0.316 and 3.16 μm/s relaxations exhibited stress drops. Note the large increase in relaxation rate at long times. (b) Frictional relaxations during $10^{4.5}$ sec holds on lizardite serpentinite gouge. Two experiments and two loading velocities are shown. Prior to the holds, sliding was unstable in experiment fr109 (top data curve) and stable in experiment fr114. (c) Examples of state-variable relaxations from experiments conducted on quartzite and granite, illustrating the effects of stable vs. stick-slip sliding prior to a hold. The hold on granite bare surfaces initiated from stable sliding and shows an initial decrease in frictional strength (reflecting the state-variable direct effect) followed by a deviation from this line caused by strengthening due to evolution of the state variables, resulting in a sigmoidal shape similar to that in the lizardite experiment. The quartzite gouge experiment was stick-slipping prior to initiation of the hold and the deviation from state-variable behavior reflects the fact that the hold initiated from the bottom of the stick-slip cycle.

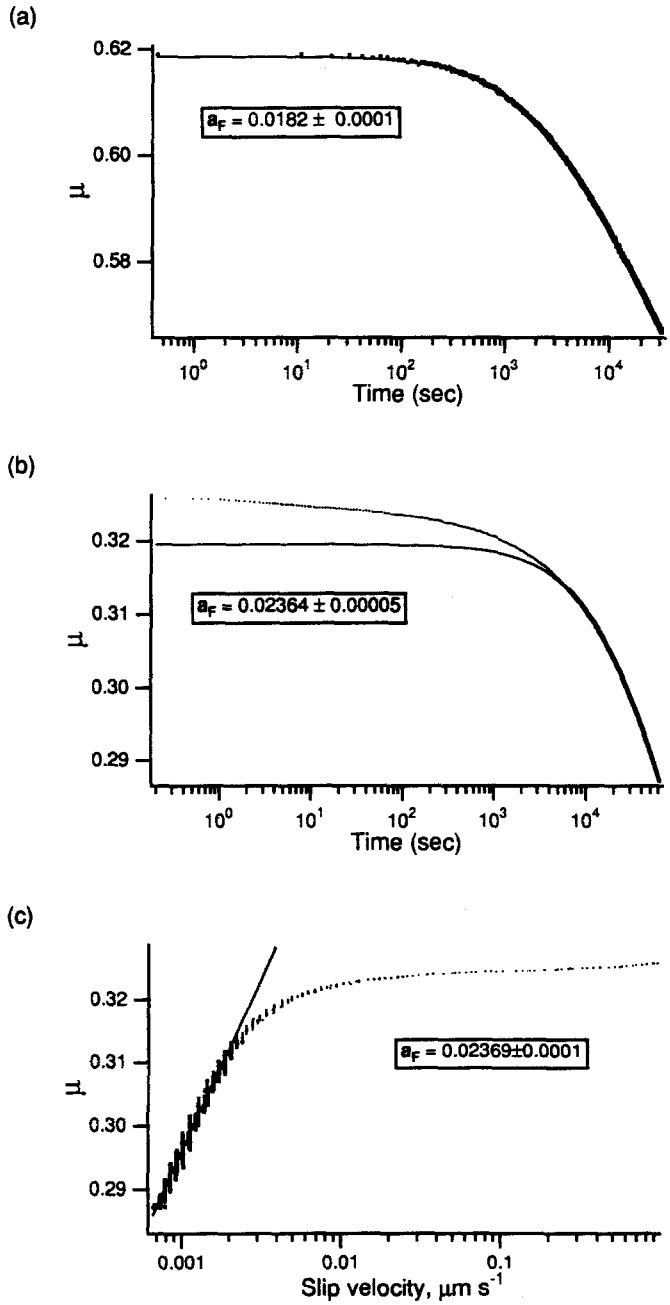
(a)
0.62
0.60
0.58
μ
a_F = 0.0182 ± 0.0001
10^0
10^1
10^2
10^3
10^4
Time (sec)
(b)
0.32
0.31
0.30
0.29
μ
a_F = 0.02364 ± 0.00005
10^0
10^1
10^2
10^3
10^4
Time (sec)
(c)
0.32
0.31
0.30
0.29
μ
a_F = 0.02369±0.0001
0.001
0.01
0.1
Slip velocity, μm s^{-1}

For the flow constitutive law, the derivative of μ with respect to ln(time) is

$$\frac{d\mu}{d\ln t} = -\mathbf{a}_F \frac{d\ln(\beta + t)}{d\ln t}. \tag{12}$$

At sufficiently long times, $kt \gg \mathbf{a}_F/V_{\text{init}}$ and

$$\frac{d\mu}{d\ln t} \cong -\mathbf{a}_F. \tag{13}$$

The slope of relaxations on a plot of μ versus ln(time) will yield the value of $\mathbf{a}_F$ directly at relaxation times much greater than β.

It is also possible to fit equation (11) to stress relaxation data as long as sliding is controlled by the flow constitutive law. This was accomplished by RUTTER *et al.* (1978) to calculate flow-law parameters for ductile rock deformation from stress relaxation experiments. However, they concentrated on a power-law model for flow, which does not fit our velocity-step data (REINEN *et al.*, 1992a; REINEN, 1993).

Figure 13a shows an antigorite gouge relaxation initiating from sliding at 0.006 μm/s, well into the flow constitutive behavior field. The model fit to the data is nearly perfect and yields a value of $\mathbf{a}_F$ of 0.0182. For slip controlled completely by the flow mechanism, there is no history dependence such as is introduced by the state variables in the state-variable constitutive law. Consequently, it is possible to apply our method for determining $\mathbf{a}_F$ to any part of a data set that is slipping sufficiently slowly to be dominated by the flow mechanism. This makes it possible to determine $\mathbf{a}_F$ from relaxations that start at velocities higher than V_{trans} using the portion of the relaxation that occurs at long times and low velocity. Figure 13b shows a determination of $\mathbf{a}_F$ (0.0236) for a relaxation initiating from sliding at 1.0 μm s^{-1} and 125 MPa normal stress on lizardite powder; this velocity was above V_{trans} and consequently the hold starts in the state-variable field. The discrepancy between the fit and the data at times less than 5000 seconds reflects the influence of the state variable mechanism; these data are excluded from the fit. At longer times, the fit is indistinguishable from the data.

Figure 13

Illustration of the methods for determining the parameter $\mathbf{a}_F$ from relaxation data. Solid lines show fits using either equation (11) (parts a and b) or equation (2) (part c). Dots are data points; in many places the dots are so numerous that they are indistinguishable. Heavy dots show data points used for fitting; light dots represent data excluded from fits. (a) Determination of $\mathbf{a}_F$ by fitting equation (11) to coefficient of friction versus time, from a hold on GC gouge at 25 MPa normal stress. The relaxation initiated at 0.006 μm s^{-1}, well into the flow regime of this material. (b) Determination of $\mathbf{a}_F$ by fitting equation (11) to coefficient of friction versus time, from a hold on T91NI6 gouge at 125 MPa normal stress. The relaxation initiated at 1.0 μm s^{-1}, well into the state-variable regime of this material. (c) Direct determination from fit of coefficient of friction versus ln(V) using the flow law (equation (2)), from the same relaxation as in part (b). Sample slip velocity was determined from slip displacement using a differencing interval of 0.1 μm.

Table 3

Comparison of values of parameter $\mathbf{a}_F$ determined from velocity steps in the flow regime and from relaxation tests initiated in the flow regime (low-V relaxation) or in the state variable regime (high-V relaxation). Values of V_i give the velocity at which relaxations were initiated. All data were determined at 25 MPa normal stress, except where noted

	Velocity steps	High-V relaxation	Low-V relaxation
Antigorite, bare	0.0157	(no data)	(no data)
	0.0186*		
	0.0181		
	0.0220		
Antigorite, powder	0.0296	0.0403 ($V_i = 0.316$)	0.0182 ($V_i = 0.0056$)
		0.0679 ($V_i = 3.16$)	
Lizardite, powder	0.0230	0.0237 ($V_i = 1.0$)†	0.0175 ($V_i = 0.0316$)
			0.0197 ($V_i = 0.0316$)†

* 100 MPa normal stress
† 125 MPa normal stress

Because the flow mechanism lacks any history dependence, the strength at all times during a relaxation controlled by the flow mechanism reflects the current slip velocity. Thus, if the sample slip velocity can be determined, $\mathbf{a}_F$ can be determined directly from the flow law (equation (2)) by a linear fit of μ versus $\ln(V)$. Such a determination is shown in Figure 13c using velocities determined with our internal resolver from the same relaxation shown in Figure 13b. As in Figure 13b, the data at early times and higher velocities reflect the influence of the state-variable mechanism, but at low velocity the data are well fit by the flow constitutive law and yield a value for $\mathbf{a}_F$ of 0.0236, in excellent agreement with the value determined by fitting equation (11) to the stress relaxation. Unfortunately, resolver data were not available during the relaxation in Figure 13a, and this method could not be applied to that case.

We have made determinations of $\mathbf{a}_F$ from both velocity-stepping experiments and relaxations and find that the values do not always agree, but do show systematic variations. Table 3 presents results for velocity steps on antigorite bare surfaces and powder and on lizardite powder done at sufficiently low velocity so that the flow mechanism should dominate. In addition, values are shown for antigorite and lizardite powder determined from relaxations initiating below V_{trans} ("Low V") and above V_{trans} ("High V"). Bare surface antigorite values from velocity steps agree well with the results from relaxations initiated at low velocity on both antigorite and lizardite, all of which cluster around 0.018, while values from velocity steps performed on powders and relaxations initiated at high velocity tend to have higher values. The higher values of $\mathbf{a}_F$ in the gouge experiments may be caused by changes in gouge textures as the deformation mechanism changes; this is described in the **Discussion** section later. Relaxations involve less total slip than do

velocity-step tests and may, therefore, give values of $\mathbf{a}_F$ that more nearly reflect the intrinsic material behavior.

Relaxation Simulations

The loading velocity prior to initiation of a hold affects the shape of the relaxation in the two-mechanism constitutive model. In Figure 14a, the simulations were generated using the same parameters used to model the bare surface antigorite serpentinite experimental velocity-step data in Figure 7. All three simulations in Figure 14a show an initial concave-up curvature reflecting the state-variable mechanism, followed by a sharp drop in frictional strength at long times, reflecting transition to flow-dominated behavior. The slope of these simulations at long times is $\mathbf{a}_F$. Since 0.32 μm/s is close to the transitional velocity, the relaxation beginning at this loading velocity undergoes the transition to flow-dominated behavior at shorter times than the relaxations initiating from faster loading velocities. Figure 14b shows the effect of loading velocity prior to a relaxation for models generated with the parameters used to model the lizardite serpentinite gouge velocity-step data in Figure 9. For all three starting velocities (Figure 14b), the initial shallow slope is followed by a strong decrease in frictional strength with log time. Like the simulations in Figure 14a, these three simulations all converge to a single line of constant slope. In the two-mechanism constitutive model with rate-strengthening state-variable behavior, all lines of constant state undergo the transition to flow-

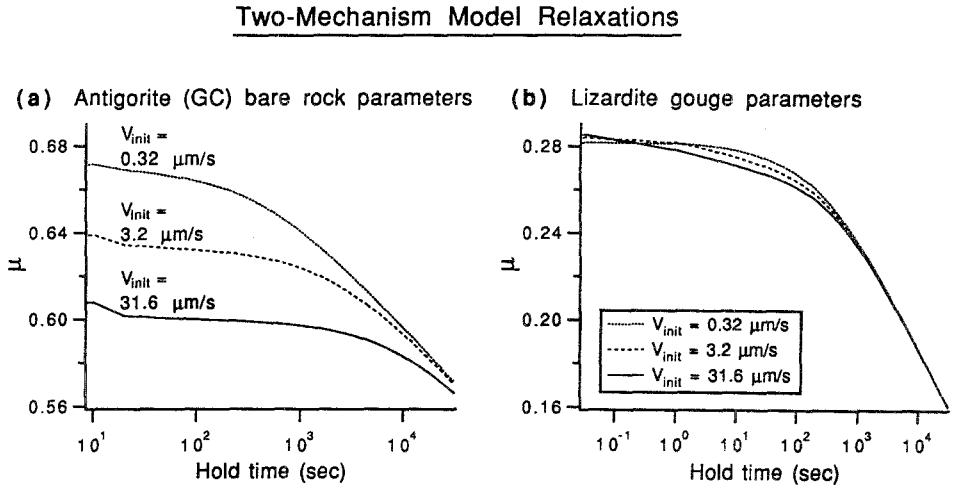

Figure 14
Model simulations illustrating the effect of loading velocity prior to a hold on the form of two-mechanism relaxations. (a) Rate-weakening state-variable law parameters. The simulations were generated with the parameters used to model the antigorite serpentinite experimental velocity-step data in Figure 7. (b) Rate-strengthening state-variable law parameters used to model the lizardite serpentinite velocity-step data in Figure 9.

dominated behavior at nearly the same velocity (see Figure 1b). This results in convergence of relaxations from different starting velocities, as exhibited by the lizardite serpentinite (Figure 12b). In contrast, antigorite serpentinite has rate-weakening state-variable behavior and lines of constant state should undergo the transition to flow-dominated behavior at very different velocities (see Figure 1a). This would result in relaxation transitions occurring at very different times depending on the initial sliding velocity (Figure 14a), as exhibited by the antigorite serpentinite (Figure 12a).

Figure 15a compares a relaxation from an experiment conducted on antigorite serpentinite gouge with simulations generated with the two-mechanism constitutive model; the relaxations all start from the same initial loading velocity (0.32 μm/s). The simulations were generated using the best-fit parameters used to model velocity-step data from experiments on both bare surfaces and gouge layers of antigorite serpentinite (Figures 7 and 8); the velocity-step data used to determine the gouge parameters are from the same experiment as the relaxation data. At short times, the experimental data have a shallow slope, most likely resulting from the low stresses in the stick-slip cycle in the gouge layer at the beginning of the relaxation; the simulations do not account for stick-slip sliding and neither simulation matches this slope well. At long times, the slopes of the simulations match the slope of the experimental data; the simulation from the gouge parameters matches the data slope better at long times than does the simulation from bare surface parameters.

Figure 15b compares relaxations from an experiment conducted on lizardite serpentinite (loading at 0.32 and 3.2 μm/s) with the simulations in Figure 14b. The

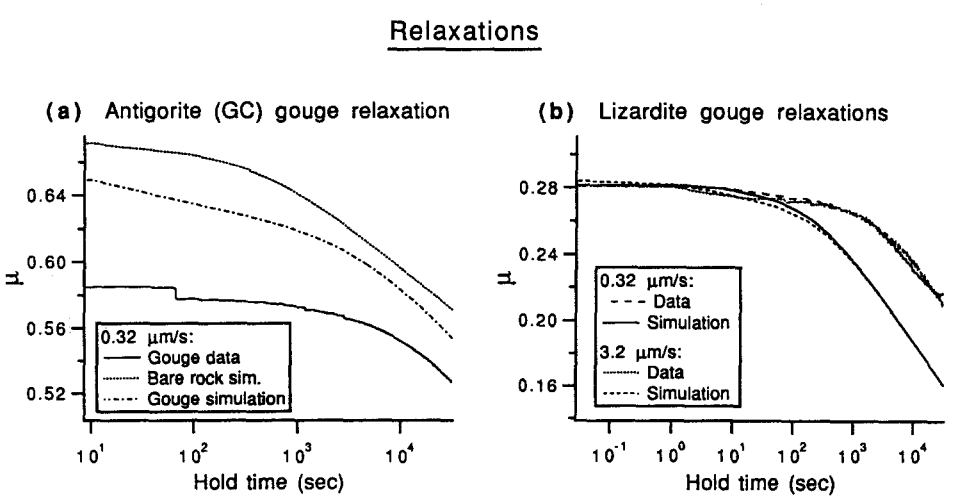

Figure 15

Comparison between relaxations of experimental data and simulations generated with parameters used to model velocity-step data; simulation parameters are listed in Table 1. (a) GC gouge relaxation. (b) T91NI6 gouge relaxations; results from two initial loading velocities are shown.

initial shallow slopes of the experimental data are well matched by the simulations, and the slope of the experimental data at long times is quite similar to the slope of the simulations. The transition in curvature takes more time in the experimental relaxations than in the model relaxations. In the simulations, the flow mechanism dominates early on as the state-variable mechanism requires continued displacement to evolve. This is consistent with the velocity-step test modeling results in which the experimental data take more time (and/or displacement) to undergo the transition between state-variable- to flow-dominated behavior than do the simulations. We are continuing to work toward understanding and correcting the misfit in the model transitional regions.

Discussion

Polymorph Effects

The major differences in frictional behavior between the antigorite and lizardite serpentinites in this study are the frictional strength and the high-velocity state-variable behavior. While bare surfaces and gouge layers of antigorite serpentinite have a coefficient of friction comparable to that for quartzo-feldspathic rocks under similar conditions, the lizardite serpentinite has a coefficient of friction less than half that of the antigorite serpentinite. This difference is probably due to the crystalline structures of the two polymorphs. The serpentine minerals are trioctahedral hydrous phyllosicates based on 1 : 1 layer structures. The dimensions of the magnesium-occupied octahedral sheet are larger than the dimensions of the silicon-occupied tetrahedral sheet, resulting in a significant misfit between the sheets (WICKS and O'HANLEY, 1988). Each polymorph represents a different solution to the misfit problem. In antigorite, the curving layers alternate, forming a corrugated morphology with the layers connected by silicon-oxygen bonds at the inflection points (Figure 16a); in lizardite, the misfit is accommodated within the planar layer producing a platy morphology with the layers connected by hydrogen bonds (Figure 16b). We expect the difference in frictional strength results from the difference in bond strengths across the serpentine layers, since hydrogen bonds are considerably weaker than Si-O bonds.

The difference in the frictional strengths of lizardite and antigorite serpentine polymorphs is presumably due to the differences in bonding strength between adjacent planar layers of the serpentine crystalline structures. In classical friction theory, the coefficient of friction is envisioned to be equal to the ratio of the shear strength to the compressive strength of the area of the contacting surfaces. The real area of contact is expected to increase with normal stress for at least two possible reasons. If the contacts undergo plastic yielding in compression, then their local compressive stress will always be equal to the compressive yield strength, and an

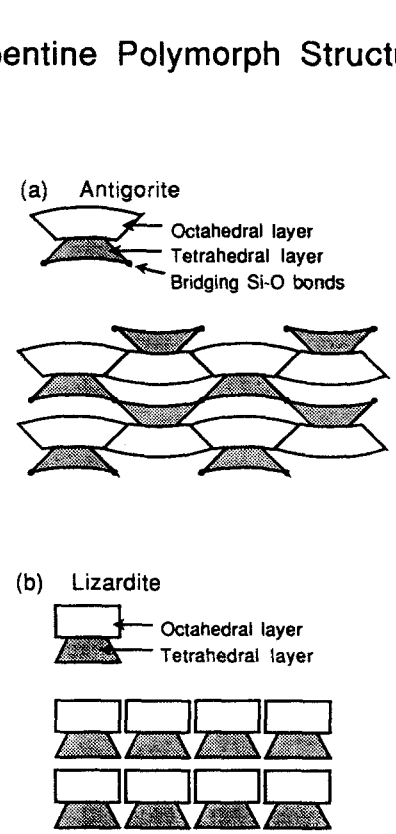

Figure 16
Schematic representations of the crystal structure of antigorite and lizardite serpentine polymorphs. (a) Antigorite structure showing the alternating curved layered structure and the Si-O bonds shared by tetrahedral layers at the changes in curvature. (b) The flat layered structure of lizardite does not have the bridging Si-O bonds of the antigorite structure.

increase in macroscopic normal stress can only be supported by a corresponding increase in contact area (BOWDEN and TABOR, 1964). Alternatively, the compressive stresses may be supported elastically, and again the total contact area is expected to be proportional to the macroscopic normal stress (GREENWOOD and WILLIAMSON, 1966). The size of the real contact areas for the two serpentine polymorphs should be similar when loaded perpendicular to the basal planes; both plastic yielding and elastic distortion involve the same basic building blocks for the two polymorphs, thus their compressive strengths should be similar. Presumably, much of the frictional shearing in serpentine occurs parallel to the basal planes. The Si-O bonds in the antigorite crystalline structure should make the shear strength of the antigorite contacts significantly higher than that of the lizardite surface contacts.

Although antigorite and lizardite have very different frictional strength, in the flow-dominated deformational regime they have the same frictional rate depen-

dence. This would occur if the frictional characteristics of antigorite result from the sum of two contributions, one which gives it considerable strength but with no rate dependence, and one (which it shares with lizardite) with less strength and a strong rate dependence. The rate dependence that they share could come from the process of shearing parallel to the layer by dislocation motion, similar to that which occurs in micas (KRONENBERG *et al.*, 1990) which lack Si-O bonds between adjacent layers. Perhaps breaking of the Si-O bonds in the antigorite is not rate-dependent because the bonds are spaced far apart in the crystalline structure, and they are broken under the applied stress without much thermal or diffusional assistance. In any case, flow-dominated frictional deformation in lizardite can be modeled by a nonlinear viscous dashpot, and in antigorite by a dashpot and slider block in parallel (see e.g., TWISS and MOORES, 1992, Figure 18.6). The rate dependence of the flow behavior is controlled by the dashpot (basal plane slip), and the strength of the antigorite by the slider (Si-O bonds). The shear strength from both of these elements would increase in direct proportion to the normal stress because higher normal stress produces larger areas of contact for bonding. Note that increasing water content causes a reduction in the strength of antigorite gouge at low velocity, with no apparent affect on the rate dependence (Figure 4). This is consistent with much of the strength coming from Si-O bonds that can become water-weakened (GRIGGS, 1967) and with the rate dependence arising from something other than the Si-O bonds.

Differences in $\mathbf{a}_F$ Determined from Velocity-step Tests and Relaxation Tests

We have determined values for $\mathbf{a}_F$ from both velocity-step tests and from relaxation tests. In each type of test, the value of $\mathbf{a}_F$ appears well constrained, but the values differ between the types of tests. In general, relaxations yield a smaller value for $\mathbf{a}_F$ than do velocity-step tests, and relaxations initiating from flow-mechanism-dominated velocities yield an even smaller value of $\mathbf{a}_F$. This is particularly true of antigorite gouge. We believe that the smaller $\mathbf{a}_F$ determined from relaxations starting from flow-dominated velocities probably represents the 'true' value of $\mathbf{a}_F$, and that the larger $\mathbf{a}_F$ values determined from other relaxations and velocity-step tests include some effects of redistribution of deformation within the gouge layer.

The frictional response of the serpentinites to sudden changes in loading velocity (whether velocity step or beginning of a relaxation) is not fully modeled by the two-mechanism constitutive model. The misfit between the model and the data might be due to an incorrect method of combining the two constitutive models. Such an explanation would result in an equal misfit with bare surface data and with gouge data; however the misfit with the gouge data is far greater than with the bare surface data. An alternate explanation for this misfit is an effect due to slip distribution within the gouge layer, not accounted for in the model. At high velocities (state-variable behavior), slip is likely to be confined to discrete planes and this "gouge effect" should be minimal, whereas at low velocities, the rate-

strengthening flow behavior may lead to more distributed deformation and the gouge effect should be more pronounced. A transition from localized to distributed slip may involve changes in frictional behavior that evolve over large displacements, such as the rounded response to velocity decreases seen in velocity steps on gouge (Figures 8 and 9).

All of our relaxation data come from experiments conducted on layers of serpentinite gouge and a "gouge effect" may be important in these tests as it appears to be in the velocity-step tests. However, the total slip at low velocity in a hold test is very small. If distribution of slip requires large displacements, then the relaxation test may be sampling a relatively constant texture, especially at the longest times and lowest velocities. For a relaxation initiated in the flow regime, slip should already be distributed, and this may explain the smaller values of $\mathbf{a}_F$ determined from these tests. This suggests that $\mathbf{a}_F$ determined from relaxations initiated at low velocity may reflect the "true" material property, while velocity steps and relaxations from high velocities may include effects of changing slip distributions within the gouge.

Experiments conducted on bare surfaces of antigorite serpentinite produce little gouge (REINEN *et al.*, 1991) and should not be influenced substantially by these gouge effects at either high or low velocities. No changes in slip distribution are expected and the flow mechanism velocity steps should exhibit only the rounding caused by machine compliance, which is accounted for by our numerical model (contrast Figure 7, bare surface antigorite, with Figures 8 and 9). Constitutive parameter determinations from bare surface experiments should yield similar values from any kind of test; unfortunately, all our relaxation tests were performed on layers of gouge and additional experiments are required to test this hypothesis.

Comparison with Other Crustal Rocks and Possible Physical Processes

Antigorite and lizardite serpentinites exhibit state-variable behavior at high experimental loading velocities; this is similar to that which is observed for other crustal rocks such as granite (DIETERICH, 1979, 1981; TULLIS and WEEKS, 1987; BIEGEL *et al.*, 1989; BEELER *et al.*, 1992), quartzite (RUINA, 1983; MARONE *et al.*, 1990; WEEKS *et al.*, 1991; WEEKS and TULLIS, 1992), and gabbro (COX, 1990). In contrast to the behavior of serpentinite, bare surfaces of granite display velocity-weakening behavior at room temperature over the range of velocities sampled in our experiments. At low experimental loading velocities, serpentinite undergoes a transition to velocity-strengthening behavior. Both this transition and the form of the frictional response of serpentinite to step changes in loading velocity are qualitatively similar to that observed in granite and quartzite under hydrothermal conditions (BLANPIED *et al.*, 1991; CHESTER and HIGGS, 1992).

Possible physical processes active in friction experiments include brittle processes, localized dislocation flow, and diffusive transfer processes. CHESTER and

HIGGS (1992) have verified through microstructural observations that the change in velocity dependence in quartzite with increasing temperature is correlated to a change in deformation mechanism. At low temperatures, cataclastic deformation dominates under dry conditions, and solution-precipitation processes dominate under hydrothermal conditions. In our room temperature experiments on serpentinite, we do not expect solution-precipitation processes to play an active role in the deformation; however, other processes may be active. Since temperature and time have the same effect on diffusive transfer processes, we expect that decreasing velocity in our experiments may activate a second deformational mechanism corresponding to increasing temperature in quartzo-feldspathic rocks. Decreasing velocity increases the time of contact of asperities on the sliding surfaces, allowing more time for deformation to occur. We believe that the most likely physical process for the flow mechanism in serpentine is dislocation glide, which has been observed in biotite at room temperature by KRONENBERG *et al.* (1990), and may be possible in other sheet silicates under similar conditions. The flow law we use is of the same form as that used by KRONENBERG *et al.* (1990) for dislocation glide in biotite (REINEN *et al.*, 1992a). Figure 17 compares the rate

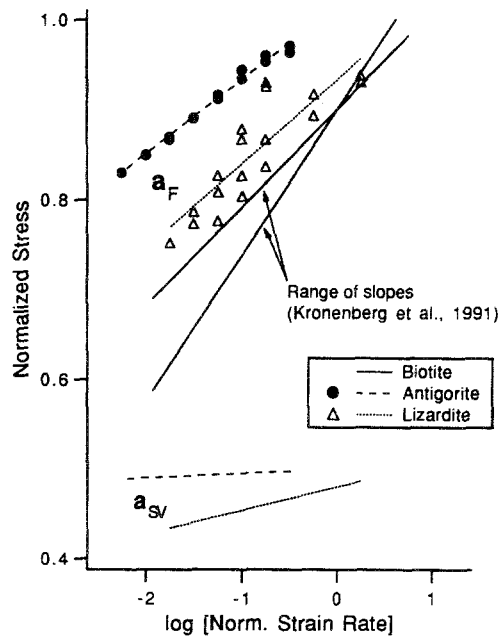

Figure 17
The rate dependence of dislocation glide in biotite compared with the rate dependence of the state-variable and flow mechanisms in serpentine. The biotite data are from KRONENBERG *et al.* (1991). For each material, the data and lines were normalized by the experimental data at the highest strain rate (or velocity); normalized results were then offset for clarity.

dependence of dislocation glide in biotite with the rate dependence of the flow mechanism in serpentinite ($\mathbf{a}_F$) as determined from velocity-step tests. The similarity of the slopes of the flow-mechanism lines and the biotite lines suggests that dislocation glide is probably responsible for the flow mechanism. These data also have implications for the origin of the state-variable mechanism. The strong difference between $\mathbf{a}_F$ and $\mathbf{a}_{SV}$ indicates that it is unlikely that the process responsible for each is dislocation glide. Fracture growth and fracture healing, both of which are time-dependent processes, are possible candidates for the state-variable constitutive behavior.

Implications for Natural Faults Containing Serpentine

The results from our study have important implications for both the strength and sliding stability of natural faults containing serpentine. The rate-strengthening nature of both serpentinites at low velocities (Figure 6) indicates that the frictional strength of the serpentinites decreases with decreasing velocities. While antigorite has a coefficient of friction similar to that of other crustal rocks, the coefficient of friction of the lizardite serpentinite is significantly lower, indicating that natural faults containing lizardite serpentine should have a shear strength less than half that expected on other crustal faults. Lizardite is the most common polymorph of serpentine identified on oceanic transform faults (e.g., AUMENTO and LOUBAT, 1971; JANECKY and SEYFRIED, 1986; PRICHARD, 1979), and its presence may explain the apparent weakness of these faults. Serpentine is common in the Franciscan rocks found along the central section of the San Andreas fault and should promote stable fault creep. If these serpentinites contain lizardite, then the low frictional strength of lizardite may explain the low stresses observed on the central section of the San Andreas fault. With modest temperature increases above room temperature, as used in our experiments, the frictional strength of lizardite could easily drop below 0.1 (REINEN *et al.*, 1993). This would obviate the need for high pore pressures to account for low stresses on the creeping section of the San Andreas fault. Low stress on fault sections that only slip seismically might result from other mechanisms that operate during dynamic slip.

In addition, alignment of the sheet-like morphology of antigorite and lizardite serpentine polymorphs may reduce the permeability of fault zones containing serpentine. This could allow for pore pressures within the fault zone to build up, effectively reducing the shear strength of the fault (e.g., BYERLEE, 1990; RICE, 1992). Aligned serpentine within a fault zone could also promote anisotropic permeability with higher values parallel to the fault and lower values across it. Such anisotropy would also help reduce the strength of the fault relative to the surrounding crust (RICE, 1992).

The transition in velocity dependence observed in our experiments indicates a transition in stability of sliding of serpentinized faults. At high velocities, the velocity

weakening behavior of the serpentinites may lead to unstable sliding (analogous to earthquakes) on serpentinized faults. The velocity-strengthening behavior observed at low velocities only results in stable sliding. Our velocity-step experiments sample loading velocities down to 0.001 μm/s, corresponding to a plate motion rate of 31.5 mm/yr; relaxation tests sample velocities down to 2×10^{-5} μm/s. Our results indicate that if slip on a fault is accommodated by frictional sliding of either antigorite or lizardite serpentinite, then only stable fault creep can occur at typical rates of plate motion. However, unstable slip may occur if the serpentinized region is forced to move at higher rates. This suggests that while serpentinized regions cannot be the site of initiation of seismic slip, seismic slip can propagate through a serpentinized region from an adjacent section of the fault.

Our reported values of frictional strength and transition velocities are bounding limits given the finite width of the deforming region in our experiments. Rate-strengthening behavior (as observed in serpentinite experiments at low velocities) leads to distributed deformation rather than shear localization. Because of the finite width of the deforming layer in our experiments, our reported values of the coefficient of friction represent an upper bound for any given relative displacement rate between two sliding blocks. In natural faults, the width of the deforming layer may be greater than the ≤ 1.0 mm represented in our experiments. Greater widths produce lower strain rates within the deforming layer. Lower strain rates for a given plate velocity should result in both lower coefficients of friction and a higher transition velocity, decreasing the strength and increasing the stable-slip velocity range of a serpentinized fault.

Conclusions

Laboratory studies of the frictional behavior of rocks can provide important information about the strength and sliding stability of natural faults. Two-mechanism constitutive models are required to describe the frictional behavior of rocks under crustal conditions. We have conducted experiments on the frictional behavior of serpentinite, a rock common to crustal faults, and we report the results of those experiments here. Our major findings described in this paper are:

1. The frictional behavior of both antigorite serpentinite and lizardite serpentinite can be modeled by a two-mechanism constitutive law combining state-variable-dominated behavior at high velocities and flow-dominated behavior at low velocities. Both rate-strengthening and rate-weakening state-variable behavior is observed in experimental velocity-step and timed-hold tests, and is described by the model.

2. The frictional strength of lizardite is very low, while that of antigorite is comparable to other crustal rocks. Small increases in temperature could result in a coefficient of friction of lizardite below 0.1. This suggests that the presence of lizardite serpentinite may account for the apparent weakness of crustal faults.

3. The low velocity data for both antigorite and lizardite serpentinites illustrates strong rate-strengthening behavior, which should lead to aseismic creep on faults containing either serpentinite.

4. Both velocity-step tests and relaxations during time-hold tests show the transition from the state-variable- to flow-dominated behavior with decreasing sliding velocity.

5. The slopes of relaxations at long times provide values of $\mathbf{a}_F$ (the flow behavior rate dependence) which are comparable to those acquired from velocity-step tests.

6. When elevated temperature is introduced as a variable, other rock types may also show two mechanism behavior. The analysis presented here for serpentinite at room temperature should be helpful in understanding the frictional behavior of many rock types.

Acknowledgments

Several people provided us with serpentinite for this study: Greg Hirth pulled the GC serpentinite out of his closet for our experiments; Don Burns and the Vermont Marble Company provided us with VM2 serpentinite; Bob Coleman suggested the New Idria source for serpentinite, and Roger Hopper and John Meyers at Calidria Asbestos Company in King City, CA allowed Terry Tullis and Connie Worthington access to the Joe Pit mine to collect the lizardite serpentinite used in this study. Nick Beeler conducted the experiments that generated the room temperature granite and quartzite data in Figure 12c. Nick, Jan Tullis, Eric Grosfils, and the Brown Tectonophysics group contributed many helpful discussions that improved an earlier version of this manuscript. Andreas Kronenberg and an anonymous reviewer provided detailed reviews that greatly improved the paper and made it substantially more tractable.

REFERENCES

ALLEN, C.R., *The tectonic environments of seismically active and inactive areas along the San Andreas fault system.* In *Proceedings of the Conference on Geologic Problems of the San Andreas Fault System* (Stanford University Press, Palo Alto, CA 1968) pp. 70–82.

AUMENTO, F., and LOUBAT, H. (1971), *The Mid-Atlantic Ridge near 45° N. XVI. Serpentinized Ultramafic Intrusions*, Can. J. Earth Sci. *8*, 631–663.

BEELER, N.M., WEEKS, J. D., and TULLIS, T.E. (1992), *Evolution of Velocity Dependence of Granite with Displacement*, EOS Trans. AGU *73*, 310.

BIEGEL, R.L., SAMMIS, C.G., and DIETERICH, J.H. (1989), *The Frictional Properties of a Simulated Gouge having a Fractal Particle Distribution*, J. Structural Geol. *11*, 827–846.

BLANPIED, M.L., and TULLIS, T.E. (1986), *The Stability and Behavior of a Frictional System with a Two State Variable Constitutive Law*, Pure and Appl. Geophys. *124*, 425–444.

BLANPIED, M.L., LOCKNER, D.A., and BYERLEE, J.D. (1991), *Fault Stability Inferred from Granite Sliding Experiments at Hydrothermal Conditions*, Geophys. Res. Lett. *18*, 609–612.

BONATTI, E., and HONNOREZ, J. (1976), *Sections of the Earth's Crust in the Equatorial Atlantic*, J. Geophys. Res. *81*, 4104–4116.

BOWDEN, F.P., and TABOR, D., *The Friction and Lubrication of Solids* (Oxford University Press, London 1964).

BYERLEE, J.D. (1990), *Friction, Overpressure and Fault Normal Compression*, Geophys. Res. Lett. *17*, 2109–2112.

CANN, J., SMITH, D.K., DOUGHERTY, M.E., LIN, J., BROOKS, B., SPENCER, S., MACLEOD, C.J., MCALLISTER, E., PASCOE, R.A., and KEETON, J.A. (1992), *Major Landslides in the MAR Median Valley, 25–30°N: Their Role in Crustal Construction and Plutonic Exposure*, EOS Trans. AGU, *73*, 569.

CHESTER, F.M., and HIGGS, N.G. (1992), *Multi-mechanism Friction Constitutive Model for Ultra-fine Quartz Gouge at Hypocentral Conditions*, J. Geophys. Res. *97*, 1859–1870.

CHESTER, F.M., and LOGAN, J.M., *Frictional faulting in polycrystalline halite: Correlation of microstructure, mechanisms of slip, and constitutive behavior.* In *The Brittle-ductile Transitions in Rocks: The Heard Volume*, Geophys. Monogr. *56* (A. G. Duba *et al.*, eds.) (AGU, Washington, D.C. 1990) pp. 49–66.

CHRISTENSEN, N. I. (1972), *The Abundance of Serpentinites in the Oceanic Crust*, J. Geology *80*, 709–719.

COX, S.J.D., *Velocity-dependent friction in a large direct shear experiment on gabbro.* In *Deformation Mechanisms, Rheology and Tectonics* (Knipe, R.J., and Rutter, E.H., eds.) (Geol. Soc. Am. Spcl. Pub. 54, 1990) pp. 63–70.

DENGO, C. A., and LOGAN, J.M. (1981), *Implications of the Mechanical and Frictional Behavior of Serpentinite to Seismogenic Faulting*, J. Geophys. Res. *86*, 10771–10782.

DIETERICH, J.H. (1972), *Time-dependent Friction in Rocks*, J. Geophys. Res. *77*, 3690–3697.

DIETERICH, J. H. (1979), *Modelling of Rock Friction: 1. Experimental Results and Constitutive Equations*, J. Geophys. Res. *84*, 2161–2168.

DIETERICH, J.H., *Constitutive properties of faults with simulated gouge.* In *Mechanical Behavior of Crustal Rocks*, Geophys. Monogr. *24* (Carter, N. L. *et al.*, eds.) (AGU, Washington, D.C. 1981) pp. 103–120.

DIETERICH, J.H., and LINKER, M.L. (1992), *Fault Stability under Conditions of Variable Normal Stress*, Geophys. Res. Lett. *19*, 1691–1694.

FROIDEVAUX, C. (1973), *Energy Dissipation and Geometric Structure at Spreading Plate Boundaries*, Earth Planet. Sci. Lett. *20*, 419–424.

GREENWOOD, J.A., and WILLIAMSON, J.B.P. (1966), *Contact of Nominally Flat Surfaces*, Proc. Royal Soc. London A *295*, 300–319.

GRIGGS, D.T. (1967), *Hydrolytic Weakening of Quartz and Other Silicates*, Royal Astron. Soc. Geophys. J. *14*, 19–31.

IRWIN, W.P., and BARNES, I. (1975), *Effect of Geologic Structure and Metamorphic Fluids on Seismic Behavior of the San Andreas Fault System in Central and Northern California*, Geology *3*, 713–716.

JANECKY, D.T., and SEYFRIED, W.E., JR. (1986), *Hydrothermal Serpentinization of Peridotite with the Oceanic Crust: Experimental Investigations of Mineralogy and Major Element Chemistry*, Geochim. et Cosmochim. Acta *50*, 1357–1378.

KRONENBERG A.K., KIRBY, S.H., and PINKSTON, J. (1990), *Basal Slip and Mechanical Anisotropy of Biotite*, J. Geophys. Res. *95*, 19,257–19,278.

KUNZE, G. (1956), *Die gewellte Struktur des Antigorits*, I. Zeit. Krist. *108*, 82–107.

LACHENBRUCH, A.H., and THOMPSON, G.A. (1972), *Oceanic Ridges and Transform Faults: Their Intersection Angles and Resistance to Plate Motion*, Earth Planet. Sci. Lett. *15*, 116–122.

MARONE, C.J., RALEIGH, C.B., and SCHOLZ, C.H. (1990), *Frictional Behavior and Constitutive Modeling of Simulated Fault Gouge*, J. Geophys. Res. *95*, 7007–7025.

MELLINI, M., and ZANAZZI, P.F. (1987), *Crystal Structures of Lizardite-1T and Lizardite-2H$_1$ from Coli, Italy*, Am. Mineral. *72*, 943–948.

PAGE, N.J., and COLEMAN, R.G., (1987), *Serpentinite Mineral Analysis and Physical Properties*, Geological Survey Research, B103–B107.

PRICHARD, H.M. (1979), *A Petrographic Study of the Process of Serpentinization in Ophiolites and the Ocean Crust*, Contrib. Mineral. Petrol. *68*, 231–241.

REINEN, L.A., TULLIS, T.E., and WEEKS, J.D. (1992a), *Two-mechanisms Model for Frictional Sliding of Serpentinite*, Geophys. Res. Lett. *19*, 1535–1538.

REINEN, L.A., TULLIS, T.E., and WEEKS, J.D. (1992b), *The Frictional Behavior of Serpentinite: Implications for Aseismic Slip on Oceanic Transform Faults*, EOS Trans. Am. Geophys. Union *73*, 550.

REINEN, L.A., WEEKS, J.D., and TULLIS, T.E. (1992c) *Interaction of Two Mechanisms during Frictional Sliding of Serpentinite*, EOS Trans. Am. Geophys. Union *73*, 310.

REINEN, L.A., WEEKS, J.D., and TULLIS, T.E. (1992d), *Comparison of the Frictional Constitutive Behavior of Antigorite and Lizardite Serpentine Polymorphs*, EOS Trans. Am. Geophys. Union *73*, 511.

REINEN, L.A., WEEKS, J.D., and TULLIS, T.E. (1992e), *Velocity Dependence of Serpentinite Friction Promotes Aseismic Slip on Faults*, Geol. Soc Am. Abstracts *24*, A323.

REINEN, L.A., WEEKS, J.D., and TULLIS, T.E. (1991), *The Frictional Behavior of Serpentinite: Implications for Aseismic Creep on Shallow Crustal Faults*, Geophys. Res. Lett. *18*, 1921–1924.

REINEN, L.A. (1993), *The Frictional Behavior of Serpentinite: Experiments, Constitutive Models, and Implications for Natural Faults*, Ph.D. Thesis, Brown University, 222 pp.

REINEN, L.A., TULLIS, T.E., and WEEKS, J.D. (1993), *A Mechanism for Weak, Creeping Faults*, EOS Trans. Am. Geophys. Union *74*, 589.

RICE, J.R., *Fault stress states, pore pressure distributions, and weakness of the San Andreas Fault.* In *Fault Mechanics and Transport Properties of Rock* (Evans, B., and Wong, T.-F. eds.) pp. 475–503 (Academic Press Ltd. 1992).

RICE, J.R., and RUINA, A.L. (1983), *Stability of Steady Frictional Slipping*, J. Appl. Mech. *105*, 343–349.

RUINA, A.L. (1983), *Slip Instability and State Variable Friction Laws*, J. Geophys. Res. *88*, 10359–10370.

RUTTER, E.H., ATKINSON, B.K., and MAINPRICE, D.H. (1978), *On the Use of the Stress Relaxation Testing Method in Studies of the Mechanical Behaviour of Geological Materials*, Geophys. J. R. Astr. Soc. *55*, 155–170.

TUCHOLKE, B.E., LIN, J., and KLEINROCK, M.C. (1992), *Crustal Structure of Spreading Segments on the Western Flank of the Mid-Atlantic Ridge at 25°25′N to 27°10′N*, EOS Trans. AGU, *73*, 537.

TULLIS, T.E. (1988), *Rock Friction Constitutive Behavior from Laboratory Experiments and its Implications for an Earthquake Prediction Field Monitoring Program*, Pure and Appl. Geophys. *126*, 555–558.

TULLIS, T.E., and WEEKS, J.D. (1986), *Constitutive Behavior and Stability of Frictional Sliding of Granite*, Pure and Appl. Geophys. *124*, 10–42.

TULLIS, T.E., and WEEKS, J.D. (1987), *Micromechanics of Frictional Resistance of Calcite*, EOS Trans. AGU *68*, 405.

TWISS, R.J., and MOORES, E.M., *Structural Geology* (W.H. Freeman and Co., New York 1992).

WEEKS, J.D. (1993), *Constitutive Laws for High Velocity Frictional Sliding and Their Influence on Stress Drop During Unstable Slip*, J. Geophys. Res. *98*, 17,637–17,648.

WEEKS, J.D., BEELER, N.M., and TULLIS, T.E. (1991), *Frictional Behavior: Glass is Like a Rock*, EOS Trans. AGU *72*, 457–458.

WEEKS, J.D., and TULLIS, T.E. (1985), *Frictional Sliding of Dolomite: A Variation in Constitutive Behavior*, J. Geophys. Res. *90*, 7821–7826.

WEEKS, J.D., and TULLIS, T.E. (1992), *High-resolution Measurement of Displacement in Rock Friction Experiments*, EOS Trans. AGU *73*, 565.

WHITTAKER, E.J.W., and ZUSSMAN, J. (1956), *The Characterization of Serpentine Minerals by X-ray Diffraction*, Mineral. Mag. XXXI, 107–126.

WICKS, F.J., and O'HANLEY, D.S. (1988), *Serpentine minerals: Structures and petrology.* In *Reviews in Min., Hydrous Phyllosilicate* (Ribbe, P.H., ed.) *19*, 91–168.

WILCOCK, W.S., PURDY, G.M., and SOLOMON, S.C. (1990), *Microearthquake Evidence for Extension across the Kane Transform Fault*, J. Geophys. Res. *95*, 15,439–15,462.

(Received August 26, 1993, revised May 25, 1994, accepted June 1, 1994)